
Acoustic backscatter by suspended cohesive sediments: field observations, Seine Estuary, France

Sahin Cihan ^{1,*}, Verney Romaric ², Sheremet Alexandru ³, Voulgaris George ⁴

¹ Department of Civil Engineering, Yildiz Technical University, Esenler, Istanbul 34210, Turkey

² IFREMER, Hydrodynamics and Sediment Dynamics Laboratory (DYNECO/PHYSED), BP 70, 29280 Plouzan, France

³ Department of Civil and Coastal Engineering, University of Florida, 365 Weil Hall, P.O. Box 116590, Gainesville, FL 32611, USA

⁴ School of the Earth, Ocean and Environment, University of South Carolina, Columbia, SC 29208, USA

* Corresponding author : Cihan Sahin, email addresses : cisahin@inm.yildiz.edu.tr ; cisahin@ufl.edu

Abstract :

Observations of suspended sediment size and concentration, flow and acoustic backscatter intensity collected on the Seine Estuary (France) are used to study the acoustic response in cohesive-sediment dominated environments. Estimates of suspended sediment concentration based on optical backscatter sensors and water samples are used to calibrate the acoustic backscatter intensity. The vertical structure of suspended sediment concentration is then estimated from acoustic backscatter information. To our knowledge, this is the first field application of the recently proposed model of acoustic scattering by flocculating suspensions based on the variation of particle density (floc-scattering model). The estimates of sediment concentration reproduce well the observations under different tidal (neap/spring) conditions, confirming the applicability of the new model in the field when detailed particle size measurements are available. When particle size measurements are not available, using estimated floc sizes based on the turbulence intensities may provide reasonable SSC profiles. During spring tide events (associated with strong currents, small flocs and large concentrations), the performances of the new floc-scattering model and the previous models given for solid particle-scattering are comparable. The floc-scattering model increases the quality of the SSC estimates especially during low-energy conditions characterized with larger flocs.

Highlights

► This is the first field application of the recently proposed model of acoustic scattering by flocculating suspensions. ► The applicability of the new model in the field is confirmed when detailed particle size measurements are available. ► When particle size measurements are not available, using estimated floc sizes based on the turbulence intensities may provide reasonable SSC profiles. ► The floc-scattering model increases the quality of the SSC estimates especially during low-energy conditions characterized with larger flocs.

20 1 Introduction

21 Suspended sediment concentration (SSC) information is essential for understanding sediment transport dy-
22 namics in estuarine and coastal environments. Acoustic profiling devices are widely used to measure both
23 current velocity and SSC profiles since, unlike the point measurements by optical systems, they can provide
24 information about the vertical structure of SSC. In sandy environments, where backscattering occurs from
25 individual particles, acoustic techniques have been used intensively to estimate the vertical distribution of
26 suspended sediment concentration and size from the backscattered signal (acoustic inversion)(e.g., Urick,
27 1948; Sheng and Hay, 1988; Downing et al., 1995; Crawford and Hay, 1993; Thorne and Hanes, 2002).
28 Transferring these techniques to cohesive sediment environments such as estuaries is challenging, because
29 cohesive sediment characteristics (size, shape, density, etc.) and flocculation are highly sensitive to flow
30 conditions (e.g., Dyer and Manning, 1999; McAnally and Mehta, 2000; Winterwerp, 2002; Voulgaris and
31 Meyers, 2004; Verney et al., 2011; Safak et al., 2013; Wang et al., 2013; Sahin, 2014). As a consequence,
32 the use of acoustic backscatter systems to study sediment transport processes in fine-grained, cohesive envi-
33 ronments is generally considered less accurate. All of the few studies published so far (e.g., Gartner, 2004;
34 Hoitink and Hoekstra, 2005; Ha et al., 2011; Sahin et al., 2013; Sahin, 2014) acknowledge the difficulty and
35 uncertainty of interpretation of the acoustic observations when sediment flocculation is present.

36 Acoustic and optical backscatter show a distinct sensitivity to flocculation. Vincent and MacDonald (2015)
37 showed that there are small but systematic decreases in the optical backscattered signal between the primary
38 and flocculated particles typically between 9% and 20% depending on the concentration. This small change
39 in backscattered signal suggests that the size of particles scattering the light (sub-particles constituting the
40 flocs) may increase a little as the degree of flocculation increases, given that the optical backscatter is in-
41 versely proportional to the particle diameter for a given mass concentration (Fugate and Friedrichs, 2002;
42 Ha et al., 2009). They conclude that the changes in the optical backscatter that occur between primary
43 (unflocculated) and flocculated particles are relatively small, from the point of view of a marine scientist
44 wishing to measure concentrations of fine sediment. Accordingly, optical instruments are commonly used
45 to measure sediment concentration in environments dominated with flocculated particles (e.g., Kineke and
46 Sternberg, 1992; Safak et al., 2013; Sahin et al., 2013; Verney et al., 2013; Sahin, 2014). In contrast, acoustic
47 backscatter intensity increases with the growth of particle (or floc). Although the signal intensity increases
48 as the floc size increases, the intensity is much smaller for flocs than that for the solid particles of same size

49 (MacDonald et al., 2013; Vincent and MacDonald, 2015). In previous studies, acoustic backscatter sensitiv-
50 ity to flocculation was related to low density of the aggregates and their porous nature (Ha et al., 2009, 2011;
51 MacDonald et al., 2013; Rouhnia et al., 2014). In ADV-based (ADV: Acoustic Doppler Velocimeter) mea-
52 surements of floc growth, Rouhnia et al. (2014) observed that the backscattered signal intensity increases
53 rapidly with floc size up to certain value, then the rate of increase significantly slows down for larger flocs.

54 The analysis of acoustic backscatter data from muddy environments is hampered by the fact that the main
55 features of scatterers are essentially unknown. It is still unclear in which form (i.e., primary particles,
56 microflocs or macroflocs) the cohesive sediment should be considered as scatterers. Most of the previous
57 studies suggest that scattering characteristics of a suspension of flocculated particles are controlled by the
58 floc properties, rather than constituent primary particles. Theoretically, the marginal value of ka (where k
59 is the wave number of the acoustic signal and a is the mean radius of scattering particle in suspension) for
60 detection of suspended sediment particles may be roughly about 0.05, suggesting that acoustical devices
61 operating at MHz frequencies would not be capable to resolve SSC well for grain sizes of order of $1\mu\text{m}$, a
62 typical primary particle size constituting flocs in muddy environments (Lynch et al., 1994; Ha et al., 2011).
63 Gartner (2004) successfully estimated concentration profiles by using flocs as scatterers with 1,200-kHz and
64 2,400-kHz acoustic Doppler current profilers (ADCP). Ha et al. (2011), using a 1,500-kHz pulse-coherent
65 acoustic Doppler profiler (PC-ADP), suggested that the acoustic signal responds to compacted and robust
66 flocs as a whole, rather than to the primary constituent particles. With a 1,500-kHz PC-ADP, inversion
67 calculations by Sahin et al. (2013) using alternatively flocs and primary particles as scatterers consistently
68 showed a better agreement for flocs, with a marginally significant correction due to primary-particle viscous
69 effect. In contrast, a study by Fugate and Friedrichs (2002) suggests that the acoustic signal may penetrate
70 the pores of flocs, and therefore the acoustic response for resuspended aggregates depends mostly on the
71 constituent grains rather than the floc characteristics. Vincent and MacDonald (2015) recently speculated
72 that the acoustic signal is sensitive to the sub-particles within the larger particles (flocs), referred to as
73 flocculi, and that the flocculi could be treated as elastic spheres with density and acoustic wave propagation
74 speeds equal to primary particles. However, the lack of field measurements of SSC and floc size with high
75 spatial and temporal resolution may have precluded previous efforts from drawing a clear conclusion. A
76 careful examination evaluating both views is warranted.

77 In the absence of a theoretical framework to describe the interactions between flocculated sediments and

78 sound, previous applications involving possible scattering by mud flocs have defaulted to using expressions
79 derived for solid (primary-particle) scatterers. Recently, MacDonald et al. (2013) carried out the first ex-
80 perimental study to investigate the interaction of sound with a suspension of flocculated sediments under
81 controlled conditions, i.e., in a homogeneous suspension with known primary and flocculated sediment size
82 and concentrations. Their results show significant differences between sediment backscattering properties
83 before, and after aggregation, suggesting that the scattering characteristics are not solely controlled by the
84 primary particles, but are also influenced by the presence of the flocs. The order-of-magnitude difference
85 between the values of scattering parameters (e.g., form function, total scattering cross-section) obtained
86 for flocs and for quartz primary particles is significant and casts doubt on the applicability of expressions
87 previously derived for solid scatterers in applications involving flocculated particles. In a complementary
88 study, Thorne et al. (2014) proposed the first model for the modification of scattering characteristics as the
89 sediment flocculates, transitioning from separate primary particles to large low-density aggregates. The ap-
90 proach models primary particles as solid elastic spheres, and large, low-density flocs as fluid elastic spheres.
91 This leads to a new model, so-called a hybrid model, that uses a variable particle density to represent the
92 processes of flocculation. The model captures well the general behavior observed by MacDonald et al.
93 (2013).

94 Here, we investigate the backscattering of the acoustic signal in a cohesive sediment environment under dif-
95 ferent hydrodynamic conditions. The field observations used here include optical and acoustic backscatter,
96 as well as floc-size measurements throughout the water column, providing a detailed synchronous picture
97 of floc variability, hydrodynamic conditions, and acoustic backscatter characteristics. This study aims to
98 test the acoustic backscatter model for flocculates of Thorne et al. (2014) and its applicability under field
99 conditions. We invert acoustic backscatter data in an estuarine environment to derive profiles of sediment
100 concentration. The implications of the results are discussed in relation to importance of floc size measure-
101 ments and improvements made by the new model over the previous solid-scatterer based models.

102 2 Method

103 2.1 Acoustic inversion

104 The backscatter intensity of an acoustic profiler can be converted to the vertical distribution of suspended
105 concentration, M , using (see Appendix)

$$M(r) = \left\{ \frac{10^{I_{dB}/20} r \psi}{k_s k_t''} \right\}^2 e^{4r\alpha}. \quad (1)$$

106 with

$$k_t'' = \left\{ \frac{3\tau c}{16} \right\}^{1/2} \frac{0.96}{ka_t} \frac{p_0}{p_{ref}}, \quad k_s(r) = \frac{\langle f_f(r) \rangle}{\sqrt{\langle a(r) \rangle \rho(a)}}, \quad (2)$$

107 where M is the mass concentration of suspended scatterers (kg m^{-3}), r is the range from the transceiver along
108 the acoustic beam (m), ψ is the dimensionless near-field correction factor describing the departure from
109 spherical spreading in the near-field of the transducer, k_s embodies the scattering properties of sediment
110 ($\text{kg}^{-1/2} \text{ m}$), k_t'' is a system constant ($\text{V m}^{3/2}$), α denotes the attenuation coefficient (Nepers m^{-1}), f_f is
111 a form function describing the backscattering characteristics of a particle relative to its geometrical size
112 (dimensionless), a is the radius of sediment in suspension (m), and $\rho(a)$ denotes sediment density (kg
113 m^{-3}). The dependency of scatterer density on particles size is used to introduce the process of flocculation
114 into the suspension scattering characteristics. The angular brackets indicate an average over the particle
115 number size distribution (mean value) present in the sample volume. In the expression for k_t , p_0 is the
116 pressure at the reference distance r_0 , which is normally defined as 1 m; the parameter τ is the acoustic pulse
117 duration, c is the speed of sound in water, k is the acoustic wave number and a_t is the radius of the active
118 area of the transducer. The range dependence of the parameters is not shown in the subsequent equations
119 for simplicity.

120 The commercial instruments used in this study (ADCP) only provide access to the processed output signal
121 in the manufacturer specified unit (counts) of received signal strength indicator. This is not a physical unit,
122 but rather a relative measure of intensity for which the reference pressure is 1 μPa at 1 m. If the ambient
123 noise intensity, E_r , is known, then the received signal intensity, E , can be converted to signal intensity I_{dB}
124 (in decibels) using the expression of Gostiaux and van Haren (2010), who corrected the initially suggested
125 formula of Deines (1999):

$$I_{dB} = 10 \log_{10} \left(10^{K_c E / 10} - 10^{K_c E_r / 10} \right), \quad (3)$$

126 where K_c is the count to decibel conversion factor (dB count⁻¹) which ranges from 0.4 to 0.5 dB count⁻¹.
 127 The value of K_c can be estimated through a calibration process in the laboratory or in the field using an
 128 empirical approach (e.g., Kim et al., 2004).

129 The attenuation coefficient $\alpha = \alpha_w + \alpha_s$ has a water component α_w and a sediment component α_s . The
 130 water component of the attenuation α_w is a function of acoustic frequency, water temperature, pressure, and
 131 salinity, that may be estimated using explicit expressions or tabulated values (e.g., Francois and Garrison,
 132 1982a, b; Kaye and Laby, 1986). The sediment attenuation term α_s can be calculated as

$$\alpha_s(r) = \frac{1}{r} \int_0^r \xi(r) M(r) dr, \quad (4)$$

133 with

$$\xi(r) = \frac{3 \langle \chi(r) \rangle}{4 \langle a(r) \rangle \rho(a)}, \quad (5)$$

134 where ξ is the sediment attenuation constant (kg⁻¹ m²), and χ is the normalized total scattering cross-
 135 section for the particles in suspension (dimensionless). The latter quantifies the scattering from a particle
 136 over all angles relative to its cross-sectional area. It also includes the effects of viscous attenuation (Thorne
 137 et al., 2014). The parameter χ consists of two components so that $\chi = \chi_s + \chi_v$. The term χ_s represents the
 138 contribution to attenuation due to scattering particles, and dominates attenuation effects for large particles.
 139 The term χ_v accounts for frictional losses due to the viscosity of the fluid surrounding the particles for $ka \ll 1$
 140 (Urick, 1948). Particle size affects strongly the relative importance of sediment attenuation components, and
 141 eventually the SSC calculations (Eq. 20).

142 In their primary unflocculated state, the particles are considered as solid elastic spheres (Eqs. 3c, 4a and 4b
 143 in Thorne et al., 2014). The model of Thorne et al. (2014) uses a modified fluid elastic sphere to characterize
 144 the scattering of large flocs with densities much closer to the density of water than that of primary particles.
 145 The intrinsic backscatter form function for an irregularly shaped fluid elastic scatterer is given as

$$f_f = \frac{k_{ff} x^2}{1 + \epsilon_1 x^2}, \quad (6)$$

146 For an irregularly shaped fluid elastic scatterer, the total normalized scattering cross-section is calculated as

$$\chi_s = \frac{k_{f\alpha} x^4}{1 - \varepsilon_2 x + \varepsilon_3 x^2 + k_{f\alpha} x^4}, \quad (7)$$

147 where $x = ka$. The values of the dimensionless fluid heuristic formulation coefficients ε_1 , ε_2 and ε_3 may
 148 depend on floc structure and the degree of variability in the coefficients should be realized with experimental
 149 studies. Here we used the values $\varepsilon_1=1.4$, $\varepsilon_2=1.5$ and $\varepsilon_3=1.0$ suggested by Thorne et al. (2014). Expressions
 150 for k_{ff} and $k_{f\alpha}$ are

$$k_{ff} = 2 \left(\frac{\gamma \zeta^2 - 1}{3\gamma \zeta^2} + \frac{\gamma - 1}{2\gamma + 1} \right), \quad k_{f\alpha} = 2 \left(\left(\frac{\gamma \zeta^2 - 1}{3\gamma \zeta^2} \right)^2 + \frac{1}{3} \left(\frac{\gamma - 1}{2\gamma + 1} \right)^2 \right). \quad (8)$$

151 The hybrid model describes the scattering properties of the primary, transitional, and flocculated scatterers
 152 using a variable size-dependent floc density and compressional velocity of sound in the scatterer. The
 153 parameter γ is the ratio of the density of the scatterer to the density of water, and ζ denotes the sound velocity
 154 ratio in the scatterer to that in the fluid. The velocity of sound within the flocs has not been measured and
 155 is not known. Here, we set this parameter to $\zeta=1.05$ (Thorne et al., 2014). The density of mud flocs, an
 156 indicator of the degree of flocculation, can be estimated as follows (Kranenburg, 1994)

$$\rho(a) = \rho_w + (\rho_s - \rho_w) \left[\frac{D_p}{D_f} \right]^{3-n_f}, \quad (9)$$

157 where $\rho(a)$, ρ_w and ρ_s are the densities of mud flocs, water and primary sediment particles, and D_f and D_p
 158 are floc and primary particle diameters, respectively. The exponent is a function of the fractal dimension n_f
 159 of the floc, which varies between 1 and 3.

160 For large low-density flocs, the model prescribes the values of the parameters f_f and χ about two orders of
 161 magnitude smaller than that of the solid particles of same size, and approach those for solid particles as the
 162 floc size decreases (or the floc density increases, Fig. 1).

163 2.2 System calibration

164 The system constant k_t'' , required for estimating SSC from time series of vertical backscatter profiles (Eq.
 165 20), does not depend on suspension characteristics and the range (Betteridge et al., 2008). Standard ap-

166 proaches to estimate k_t'' involve special laboratory equipment and setup either for full electronic and acous-
 167 tic calibration of the system, or for conducting extensive measurements in a homogeneous suspension with
 168 known sediment concentrations and scattering characteristics (Thorne and Hanes, 2002). In the absence
 169 of the means to perform these tests, Sahin et al. (2013) recently suggested a simpler alternative approach
 170 based on field data that does not require an extensive laboratory setup. The method is akin to an inverse
 171 modeling approach, based on synchronous, independent measurements of SSC, e.g., obtained with an OBS,
 172 and sediment sizes throughout the water column. The proposed approach searches for the value of k_t'' that
 173 minimizes the RMS error between a selected set of optical SSC observations and estimates:

$$\varepsilon = \sqrt{\frac{1}{qN} \sum_{i=1}^q \sum_{j=1}^N (M_O^{i,j} - M_A^{i,j})^2}, \quad (10)$$

174 where q is the number of vertical levels at which optical measurements of sediment concentration are avail-
 175 able, N is the number of observations in the concentration time series, $M_A^{i,j}$ is the estimated (based on the
 176 acoustic backscatter) and $M_O^{i,j}$ is the measured sediment concentration at the location of i th OBS level in j th
 177 measurement interval. The count to decibel conversion factor K_c needs to be determined in order to calculate
 178 $M_A^{i,j}$ through Eqs. 3 and 1. A detailed explanation of the procedure to estimate K_c can be found in Kim et
 179 al. (2004).

180 3 Field experiment

181 3.1 Site and instrumentation

182 The observations were made in the lower part of the Seine Estuary, France, within the estuarine turbidity
 183 maximum (TM) in spring and autumn of 2011 during the EC2CO/Seine Aval FLUMES Experiment, ded-
 184 icated to the investigation of suspended sediment dynamics in key compartments within the estuary (Fig.
 185 2). The Seine Estuary is a macrotidal system flowing into the English Channel through a shallow bay. The
 186 farthest upstream extent of the turbidity maximum is located about 60 km inland, corresponding to low river
 187 flow during spring tide conditions. During periods of high freshwater discharge ($> 1,000 \text{ m}^3/\text{s}$), the turbidity
 188 maximum zone is flushed out of the estuary mouth into Seine Bay (Verney et al., 2009). The diurnal tidal
 189 range at the estuary mouth varies between 3 m and 8 m corresponding to neap and spring tides, respectively

190 (Table 1), with the tidal range of less than 1 m at the upstream limit of the estuary, penetrating a distance
191 of 160 km inland (limited by a weir) (Verney et al., 2009). The flood-dominated tidal flow is asymmetric,
192 characterized by longer ebb duration than flood duration, inducing higher flood velocities than ebb veloc-
193 ities. The deformation of the tidal wave also induces an asymmetry between slacks duration, i.e., longer
194 high water slack than the low water slack (Brenon and Le Hir, 1999). Tidal currents largely control fine
195 particle resuspension within the TM, with higher resuspension rates during spring tides than on neap tides
196 (Brenon and Le Hir, 1999; Uncles et al., 2002; Deloffre et al., 2006). The river flow also plays an impor-
197 tant role in controlling sediment dynamics of the TM. River discharge varies between 100 m³/s in summer
198 and more than 2,200 m³/s in winter, with the mean discharge of approximately 410 m³/s. (Guezenc et al.,
199 1999). During high river discharge periods, the bulk of the fine sediment fraction is deposited in the subtidal
200 areas seaward of the mouth. During low river discharge periods, these fine sediments are resuspended by
201 wind-induced waves and spring tide flood currents, and a part of them are transported back into the lower
202 estuary by flood tidal currents (Deloffre et al., 2006).

203 Hydrodynamics and suspended sediment characteristics were monitored during different tidal cycles at ap-
204 proximately 9 m water depth (Fig. 2), using a cluster of acoustic and optical instruments. A downward
205 looking ADCP, mounted on a floating platform, collected current and backscatter data continuously through-
206 out the water column. Current profiles were sampled at 1 Hz and recorded as 2 min ensemble averages in
207 20 cm vertical bins, with the first bin centered at about 1 m below the sea surface. A LISST-100X (Laser
208 In Situ Scattering Transmissometer, Sequoia Scientific) and an OBS-3 (Optical Backscatterance Sensor,
209 Campbell Scientific) were deployed on a profiling frame, observing the whole water column every 15 min.
210 The LISST estimated size distributions of suspended particles at 32 class ranges between 2.5 and 500 μm
211 at 1 Hz samples with a path reduction module of 80% (i.e., 1 cm path length), and the data were processed
212 in 50 cm vertical bins. The OBS, processed in 10 cm bins, sampled the turbidity at 2 Hz. Water samples
213 (from the surface and the bottom), collected every hour, were used to estimate de-flocculated particle size
214 distributions, and for mass concentrations for calibration of the optical sensor. The OBS was re-calibrated
215 with water samples for each data set with good linear regressions (Fig. 3). The variability of the slopes
216 of the calibration curves seems to be associated with variable neap/spring conditions causing differences
217 in floc packing and hence floc density. Further analysis to explain such variability is in progress, and the
218 details will be presented elsewhere (Verney et al., in preparation). Calibration curves show no clear relation

219 between flocculation level and the slope for each data set, justifying the negligible dependency of the OBS output
220 signal on flocculation level. The OBS observations will be considered throughout this study as reference
221 SSC measurements.

222 3.2 Observations

223 Fig. 4 shows an example for the grain size distributions measured by the LISST (spring tide in Novem-
224 ber 2011) represented as both volume size distributions and number size distributions. When represented
225 as volume size distributions (Fig. 4a), the LISST-derived grain sizes exhibit a bimodal distributions with
226 modes positioning around $50 \mu\text{m}$ and $250 \mu\text{m}$. Since the positions of the peaks are consistently larger than
227 the median size of the de-flocculated volume particle size distribution ($D_{50}=9 \mu\text{m}$, Fig. 5), we interpret this
228 to indicate the presence of flocculated sediment (floc mode, Verney et al., 2013). Conversion from volume
229 fraction to number fraction distributions results in much narrower distributions with a single mode at con-
230 sistent smaller than $10 \mu\text{m}$ (Fig. 4b). This indicates that the existence of a few number of large flocs does
231 not significantly affect the number distribution but dominates the volume distribution due the large volume
232 they occupy. This behavior was consistently observed through the entire data sets analyzed and is consistent
233 with the previous observations made in fine-sediment environments (Moore et al., 2012). Between 8:00 and
234 13:00 hours, existence of a larger mode than the rest of the data set in the number distribution is probably due
235 to calmer flow conditions and lower sediment concentrations that are favorable to flocculation in energetic
236 environments such as the Seine Estuary (Fig. 4b). We will refer to LISST mean floc size estimates over
237 particle volume and number size distributions as D_{mv} and D_{mn} , respectively. In order to match the particle
238 size definition in the acoustic/SSC conversion method (Section 2.1), we represent the measured flocs by the
239 mean values over LISST particle number size distributions (D_{mn}) in the remainder of this paper. This is also
240 consistent with the concept of scattering from the tightly-bound flocculi by Vincent and MacDonald (2015).

241 Data collection during spring tide on May 18th (Figs. 6a-d) is characterized by two periods of strong current
242 activity (exceeding 2 m/s) during early flood and early ebb; the first occurred between 07:30 to 09:30 hours,
243 and the second, exhibiting slightly weaker velocities, occurred between 13:30 to 16:00 hours (Fig. 6a).
244 During these periods, a strong acoustic backscatter is recorded, suggesting the presence of large amounts
245 of suspended matter in the water column (Fig. 6b). Qualitatively, the strength of the ADCP backscatter
246 signal agrees with the fluctuations of OBS observations. SSC up to 2 kg/m^3 is observed before 7:00 hours,

247 which settles for an hour with the weak currents. During flood (starting after 7:30 hours), freshly settled
248 sediments from the previous tidal cycle are picked up by the flow (Fig. 6c). During this period, suspended
249 particles are composed mainly of small flocs ($D_{mn} \simeq 5 \mu\text{m}$, $D_{mv} \simeq 50 \mu\text{m}$, Fig. 6d). As the current speed
250 decreases toward the late flood, hydrodynamic conditions become favorable to flocculation, and sediments in
251 suspension start to settle. During this period, flocs with D_{mn} around $10 \mu\text{m}$ ($D_{mv} \simeq 100 \mu\text{m}$) were observed
252 to form throughout the water column. With the start of the ebb cycle at 14:00 hours, SSC starts increasing
253 again, dominated by small flocs and associated with the flushing of the TM to the estuary.

254 Throughout the neap tide on May 23rd, suspended sediments respond to the hydrodynamic forcing in a
255 similar manner. The intense current activity periods observed during flood and ebb are weaker than during
256 spring tides with flow speeds less than 2 m/s (Fig. 6e). During these periods (between 6:50-9:30 hours, and
257 11:00-13:30 hours), the SSC reaches up to 2 kg/m^3 near the bed (Fig. 6g), in agreement with the strong
258 acoustic reflections recorded by the ADCP (Fig. 6f). Suspended sediments are mainly small flocs during
259 these energetic periods, probably due to strong turbulence causing floc breakage. However, conditions are
260 ideal for floc growth during slack water, with flocs larger than $10 \mu\text{m}$ ($D_{mv} \simeq 100 \mu\text{m}$) spanning the entire
261 water column (Fig. 6h).

262 Observations made in November 2011 during neap (Fig. 7a-d) and spring tides (Fig. 7e-h) are character-
263 ized by weaker currents than those observed in May. While sediment responds similarly to hydrodynamic
264 forcing, the measured flocs are slightly larger than those measured in May, related to the lower turbulence
265 intensity corresponding to the weaker currents.

266 **4 Results and discussion**

267 **4.1 Calibration and model performance with measured floc sizes**

268 For calibration of the approach presented in Section 2.2, the observations collected on November 10th are
269 presented here, and the other sets were used to validate the results. The independent calibration checks with
270 the other data sets resulted in similar calibration constants, ensuring the reliability of the calibration. The
271 calculations were performed using the LISST D_{mn} (Fig. 7h) and corresponding densities (Eq. 9), taking
272 both sediment and water attenuation into account through Eqs. 5-9. A constant value $n_f = 2$, typical for
273 an estuarine floc (Kranenburg, 1994), was used in the calculations here. This value is consistent with the

274 flocc structural analysis made using the measurements of volume concentrations from LISST and the mass
 275 concentrations from OBS to estimate density and fractal dimensions of the flocs (Verney et al., 2013). The
 276 detailed investigation on the relation between the hydrodynamic forcing and the flocc structure are beyond the
 277 scope of this paper, and the related results will be presented in detail elsewhere (Verney et al., in preparation).
 278 The sensitivity of the acoustic SSC estimates on the fractal structure is discussed in Section 4.4. Count to
 279 decibel conversion factor as well as the noise levels for each transducer of the ADCP employed in this study
 280 were determined in the laboratory ($K_c=0.43$ dB/count and $E_r=46$ counts in Eq.3).

281 In order to ensure the independence of k_t'' on suspension conditions, SSC measurements were divided into
 282 groups of 0.1 kg/m^3 (Fig. 8a), and for each group, the optimum k_t'' giving the minimum difference between
 283 measurements and calculations was determined (Eq. 10, Fig. 8b). The value of k_t'' for different SSC classes
 284 does not show a systematic variation, and approximately 90% of the k_t'' values lie within the $\pm 30\%$ of the
 285 average value, corresponding approximately to the standard deviation (circles and the solid line in Fig. 8b).
 286 Variation of k_t'' with range is seen in Fig. 8c for each meter from the instrument. Consistent with the SSC
 287 dependency, no systematic variation is apparent. Therefore, this consistent mean value of k_t'' was used as an
 288 instrument constant in the analyses.

289 The performance of the ADCP to estimate the values of SSC is presented in Figs. 9 and 10 for the data sets
 290 in May and November, respectively. The vertical profiles of SSC estimated from acoustic backscatter show
 291 a good agreement with the OBS-3 observations for different data sets, with correlation coefficients varying
 292 between $r=0.77$ and $r=0.90$ ($r_{average}=0.83$) and RMS errors between $\varepsilon=0.12 \text{ kg/m}^3$ and $\varepsilon=0.17 \text{ kg/m}^3$
 293 ($\varepsilon_{average}=0.14 \text{ kg/m}^3$). These results indicate that the newly proposed variable-density flocc scatterer model
 294 (hybrid model) of Thorne et al. (2014) shows a good performance under both low and high concentration
 295 conditions during different tidal cycles, when used in conjunction with vertical mean flocc size profiles (over
 296 the particle number distributions) estimated by the LISST.

297 **4.2 Model performance with estimated flocc sizes**

298 Application of the method to estimate SSC profiles (Section 2.1) requires information on the vertical dis-
 299 tribution of the mean sediment size (flocc size), in addition to the backscatter intensity profiles. While com-
 300 mercial current profilers are commonly used to measure current and backscatter intensity profiles, flocc size
 301 measurements with high vertical resolution are not practical for long periods.

302 It is known that floc formation is dominantly controlled by flow turbulence and sediment availability (e.g.,
 303 McCave, 1984; Dyer and Manning, 1999; Hill et al., 2001; Winterwerp, 2002; Verney et al., 2009; Safak
 304 et al., 2013; Sahin, 2014). Therefore, floc size profiles may be estimated from turbulence intensity profiles
 305 extracted from the current velocity profiles when detailed sediment size measurements are not available.

306 The effect of turbulence on floc formation can be represented by the shear rate G (s^{-1}) (Berhane et al., 1997;
 307 Dyer and Manning, 1999; Safak et al., 2013; Sahin, 2014)

$$G = \left(\frac{\varepsilon}{\nu} \right)^{1/2}, \quad (11)$$

308 where $\varepsilon = \frac{u_*^3}{\kappa z}$ is the dissipation rate with u_* the friction velocity, $\kappa=0.41$ the von Karman's constant and z
 309 the distance above bed. Assume a logarithmic law of the wall for unstratified turbulent boundary layer

$$u(z) = \frac{u_*}{\kappa} \ln \left(\frac{z}{z_0} \right), \quad (12)$$

310 where u is the horizontal velocity, and z_0 is a function of bottom roughness at which the velocity is zero.
 311 The parameters u_* and z_0 in Eq. 12 can be estimated iteratively based on the values providing the best-fit
 312 between logarithmic profiles and the measured current velocity profiles $u(z)$ outside the wave boundary layer
 313 (Lacy et al., 2005; Safak et al., 2013). This procedure was applied to the ADCP velocity profiles in order
 314 to calculate the friction velocities for all the data sets. The valid logarithmic zone spanned the entire profile
 315 for about 75% of the measurement bursts. The u_* estimates were then used to calculate the dissipation rate
 316 and the shear rate throughout the vertical axis using Eq. 11.

317 Relationship between the calculated shear rates and the LISST floc sizes (D_{mn}) is presented in Fig. 11. Flocs
 318 of around $10 \mu\text{m}$ has the largest frequency of occurrences at $G \simeq 1 \text{ s}^{-1}$. For higher shear rates, the frequency
 319 of occurrences of smaller flocs begin to increase (Fig. 11a). For all data sets, floc size shows an increasing
 320 trend with increasing shear rate up to $\sim 1 \text{ s}^{-1}$. This trend is reversed for larger shear rate values, and the
 321 floc size starts decreasing with increasing shear rate up to $\sim 13 \text{ s}^{-1}$. Floc size maintains a constant value of
 322 around $5 \mu\text{m}$ at higher shear rates (Fig. 11b). The floc size-shear rate relationships shown in the Fig. 11 is
 323 consistent with the previous studies (e.g., Berhane et al., 1997; Dyer, 1989; Sahin, 2014), and it allows for
 324 estimation of the floc size profiles when detailed sediment size measurements are not available.

325 The floc size profiles estimated using the relationship shown in Fig. 11b (thick blue curve) are in good

326 agreement between the mean floc sizes measured by the LISST, with RMS errors ranging from 1.6 microns
 327 to 2.2 microns for different data sets (Figs. 12-13a and b). Resulting SSC values are in the same range as the
 328 data, and represent well the time evolution of the measurements. Average RMS error increases slightly from
 329 0.14 kg/m^3 to 0.17 kg/m^3 when the estimated floc sizes are used instead of the measured ones to estimate
 330 SSC profiles. These findings indicate that using estimated floc sizes in calculations can provide reasonable
 331 SSC profiles when detailed floc size measurements are not available.

332 4.3 Previous models for solid scatterers

333 Mean floc sizes over particle number size distributions exhibit values lower than $15 \mu\text{m}$ throughout the water
 334 column during different tidal cycles (Figs. 6d, h; and 7d, h). Based on the model of Thorne et al. (2014),
 335 although the scattering properties (represented by the parameter k_s) of large flocs may be significantly dif-
 336 ferent from those of the solid particles, the values of k_s reconcile as the particle size decreases (Fig. 14).
 337 For the mean floc size (D_{mn}) range observed here, k_s values for flocs (k_{sf}) maintain values close to those
 338 (less than three times difference) of solid scatterers (k_{ss}), suggesting that the previous models based on the
 339 solid particle-scatterer assumption may also provide acceptable results when used with the measured flocs.
 340 To test this, we repeated the calculations using the expressions given by Moate and Thorne (2013) for sandy
 341 particles (assuming a constant density, $\rho = 2650 \text{ kg/m}^3$). The solid particle-scatterer model also performs
 342 satisfactory during energetic periods (during flood and ebb), when D_{mn} is consistently lower than $5 \mu\text{m}$,
 343 during both Neap (Fig. 15a-d) and Spring tides (Fig. 15a-d) in November. During these high concentration
 344 periods, the new hybrid model (floc-scatterer model) predicts the SSC values with 0.19 kg/m^3 RMS error
 345 on average, while the error is 0.20 kg/m^3 for the solid-scatterer model. For this particle size range, the scat-
 346 tering characteristics of solid particles and flocs become remarkably close with the ratio k_{ss}/k_{sf} less than
 347 1.5. During the periods characterized with lower concentrations and larger flocs (during slack), difference
 348 between the scattering properties is larger ($k_{ss}/k_{sf} \sim 3$), and the solid particle-scatterer model consistently
 349 underestimates the concentrations while the hybrid model is able to reconstruct well the SSC profiles. Dur-
 350 ing these periods, the RMS errors for the hybrid and the solid-scatterer models are 0.02 kg/m^3 and 0.042
 351 kg/m^3 , respectively. The percentage errors demonstrate more clearly the performances of these two models
 352 due to large differences between concentrations during flood/ebb (high-concentration) and slack water (low-
 353 concentration) conditions (Figs. 15e and 16e). While the hybrid model predicts high and low concentrations

354 with around 10% and 18% errors (average of all the data sets), respectively, the solid-scatterer model's per-
355 formance is significantly different under high concentration (small-floc) and low-concentration (large-floc)
356 conditions with 15% and 40% errors, respectively.

357 In terms of mass sediment fluxes (per unit width), determined by integrating the product of velocity and SSC
358 data over the depth of the water column, floc-scatterer model performs better than the solid-scatterer model
359 under both low and high energy conditions (Figs. 15f and 16f). The percentage errors in flux estimates
360 yield similar values to those obtained for the SSC estimates (Figs. 15e and 16e). The tidally averaged RMS
361 errors are 2 kg/m/s and 3.4 kg/m/s for floc-scatterer and solid-scatterer models, respectively. The sediment
362 flux values are remarkably low during low energy periods characterized with large flocs, where the the floc-
363 scatterer model's performance is significantly better than the previous solid-scatterer model. On average,
364 the sediment flux values during these low energy periods are about 10 times lower than the values during
365 high energy periods. While the percentage error between the two alternative methods are considerably high
366 during these periods, the difference in sediment fluxes is negligibly low due to lack of both high velocities
367 and SSCs.

368 These results suggest that previous models given for solid particles may perform closer to the variable den-
369 sity floc model during energetic events associated with strong currents, small flocs and large concentrations.
370 This is because of the fact that mean floc size values become very low ($D_{mn} \simeq 5 \mu\text{m}$) when they are repre-
371 sented by the particle number distributions under field conditions in muddy environments. The improvement
372 made by the new floc-scatterer model is much more apparent during less energetic periods characterized by
373 larger flocs. However, the contribution of the sediment suspended during these less energetic periods to the
374 total sediment flux may be considered negligible.

375 **4.4 Sensitivity to fractal structure**

376 The fractal dimension was assumed constant and set to $n_f=2$, a typical value for an estuarine floc. The value
377 of the fractal dimension may change from 1.4 for very fragile flocs to larger than 2.2 for strong estuarine
378 flocs (Kranenburg, 1994). Based on field measurements in estuarine environments and on intertidal mudflats,
379 Dyer and Manning (1999) show that the value of the fractal dimension depends strongly on flow conditions
380 and suspended sediment concentration. The floc fractal structure affects the important floc characteristics
381 such as the floc density and strength, and the collision-induced shear stresses. In order to investigate the

382 sensitivity of the inversion algorithm to the value of the fractal dimension, calculations were repeated using
383 the measured floc sizes with different fractal dimensions $n_f=1.5$ and $n_f=2.3$. Fig. 17 shows the relation
384 between the measured SSC and the estimated ones using different fractal dimensions during neap tide in
385 November (November 3rd). The model with $n_f=2$ underestimates SSC for low concentrations (i.e., below
386 0.2 kg/m^3) and overestimates SSC for high concentration conditions (i.e., above 1 kg/m^3). The model with
387 $n_f=1.5$ performs better at low concentrations, while the model with $n_f=2.3$ reconstruct the observations
388 well when the SSC is high. In other words, the model with increasing fractal dimension performs better
389 as the concentration increases. This behavior is consistent with the concept of a cohesive sediment particle
390 undergoing aggregation processes. Our observations suggest a negative correlation between SSC and the
391 floc size (Figs. 6 and 7). Low concentrations indicate the existence of larger but more fragile flocs, which
392 are expected to have lower fractal dimensions. More robust smaller flocs observed during energetic, high-
393 concentration conditions are typically have larger fractal dimensions (Kranenburg, 1994). This behavior
394 can also be explained by the dependence of floc density on the fractal dimension. According to Eq. 9, floc
395 density scales with $D_f^{n_f-3}$. Hence, for a constant floc size, floc density increases with increasing fractal
396 dimension resulting in an increase in f_f (or the acoustic sensitivity, Fig. 1), and therefore in k_s (Eq. 14).
397 Based on Eq. 20, increasing k_s yields lower SSC estimates. Consequently, using larger fractal dimensions
398 in the model results in lower concentration estimates.. Although the results presented here do not suggest
399 a significant dependence on fractal dimension, they highlight that using a variable fractal dimension may
400 increase the quality of the estimates.

401 5 Conclusions

402 Observations of the vertical profiles of SSC, floc size, and the backscatter intensity of the acoustic signal
403 collected in the lower part of the Seine Estuary (France) during May and November 2011, covering both
404 neap and spring tides were used to study the behavior of the acoustic signal of suspended cohesive particles.
405 In addition to the acoustic backscatter profiles, the OBS and the LISST provided direct SSC (sometimes
406 exceeding 2 kg/m^3) and floc size measurements within the entire water column, respectively. The vertical
407 distribution of observations provides a detailed basis of comparison and validation of the results of backscat-
408 ter analysis and interpretation. The newly proposed hybrid model (Thorne et al., 2014), which is based on
409 variable particle density to describe the scattering of flocculated sediments, is tested to calculate the scat-

410 tering parameters needed to estimate the SSC profiles, for the first time in a field application. The resulting
411 SSC profiles are in agreement with the OBS point measurements under a variety of field conditions, con-
412 firming the applicability of the new hybrid model in the field when detailed particle size measurements are
413 available.

414 The model requires information on the vertical distribution of the mean sediment size (floc size), which is
415 difficult to measure, and mostly unavailable over long periods. Since floc growth and breakage are controlled
416 by the flow turbulence level, floc sizes may be estimated under known turbulence conditions. Turbulent shear
417 profiles were estimated using the current velocity profiles measured by the ADCP. The friction velocities
418 were estimated by fitting the logarithmic profiles in a least-square sense to the current velocity profiles,
419 outside the wave boundary layer, which can then be used to approximate the dissipation of turbulent kinetic
420 energy and the turbulent shear profiles. The relationship observed between the shear rate and the floc size
421 allows for estimation of floc sizes based on the flow conditions. Using estimated floc sizes in calculations
422 provide reasonable SSC profiles when detailed floc size measurements are not available.

423 Sediment size is defined by the mean value over the particle number size distribution in the model. The
424 mean floc size values over particle number size distributions are consistently lower $15 \mu\text{m}$ throughout the
425 water column. During energetic events associated with strong currents, the observed floc sizes are around
426 $5 \mu\text{m}$, for which the scattering properties of flocs and the solid particles are remarkably close. Therefore,
427 previous models given for solid particles perform almost as well as the variable density floc model during
428 these periods. The improvement made by the new floc-scatterer model is apparent during less energetic
429 periods characterized by larger flocs, as the floc scattering properties differ from those of solid particles
430 with increasing sediment size. This result is probably universal since previous observations in different
431 geographical locations indicate a similar mean sediment size range, when represented by the particle number
432 size distributions (e.g., The Romans-sur-Isre, France (Moore et al., 2012); Atchafalaya Shelf, Gulf of Mexico
433 (Safak et al., 2010)).

434 The observations and the results obtained at a fixed geographic location during different tidal cycles are
435 consistent. Some of the errors in SSC estimates can be attributed to the uncertainties related to the refer-
436 ence estimates of SSC profiles based on OBS data and uncertainties related to the particle size and density
437 estimates based on shear rate profiles. Salinity-induced stratification, which is likely to be strongest during
438 the transition between flood and ebb tides, might affect the results inferred here, since it is likely to have

439 an effect on flocc dynamics, overall backscatter from the ADCP, and the shear stress estimated from the
 440 logarithmic profiles. The site-dependence should also be investigated since the flocs of the same size may
 441 have different densities depending on the sediment characteristics of the site (e.g., organic content, fractal
 442 dimension). Other parameters affecting the flocc scattering characteristics, i.e., fluid heuristic formulation
 443 coefficients, sound velocity in a fluid scatterer and in primary particles, were set to constant values used by
 444 MacDonald et al. (2013) and Thorne et al. (2014). Future efforts should focus on validation of the acous-
 445 tic behavior inferred here with as many supporting measurements as possible to constrain the model input
 446 parameters at different locations under different conditions.

447 Appendix

448 Under incoherent scattering conditions, the root-mean-square backscattered voltage $V(r)$, at range r , from
 449 a piston transceiver, can be written as (Sheng and Hay, 1988; Hay and Sheng, 1992; Thorne et al., 1993;
 450 Thorne and Hanes, 2002; Moore et al., 2012),

$$V(r) = \frac{k_s(r)k_t}{r\psi(r)}M(r)^{1/2}e^{-2r\alpha}, \quad (13)$$

451 with

$$k_t = RT_v p_0 r_0 \left\{ \frac{3\tau c}{16} \right\}^{1/2} \frac{0.96}{ka_t}, \quad k_s(r) = \frac{\langle f_f(r) \rangle}{\sqrt{\langle a(r) \rangle \rho(a)}}, \quad (14)$$

452 where R is the transducer receive sensitivity, T_v is the voltage transfer function of the system. Eq.13 can be
 453 rearranged in terms of pressure using the relationship $V = RT_v p_{rms}$, where p_{rms} is the the root-mean-square
 454 backscattered pressure (Moore et al., 2012),

$$p_{rms} = p_0 r_0 \frac{k_s k'_t}{r\psi} M^{1/2} e^{-2r\alpha}, \quad (15)$$

455 where

$$k'_t = \left\{ \frac{3\tau c}{16} \right\}^{1/2} \frac{0.96}{ka_t}. \quad (16)$$

456 Sound pressure level in decibels can be determined using

$$I_{dB} = 20 \log_{10} \left(\frac{p_{rms}}{p_{ref}} \right), \quad (17)$$

457 where p_{ref} is the reference pressure at a reference distance r_0 (for the instrument used in this study, ADCP,
458 $p_{ref} = 1 \mu\text{Pa}$ and $r_0 = 1 \text{ m}$) Substituting Eq. 15 into Eq. 17 yields

$$I_{dB} = 10 \log_{10} \left(\frac{p_0^2}{p_{ref}^2} \frac{k_s^2 k_t'^2}{\psi^2 r^2} M e^{-4r\alpha} \right) = 10 \log_{10} \left(\frac{p_0^2}{p_{ref}^2} \right) + 10 \log_{10} \left(\frac{k_s^2 k_t'^2}{\psi^2 r^2} M e^{-4r\alpha} \right). \quad (18)$$

459 The first term on the RHS is the term commonly referred to as the source level, which is the intensity of
460 emitted signal. The absolute level of the source level SL (in dB, i.e. the transmitted power) is also rarely
461 known accurately (e.g., Holdaway et. al., 1999). Since it is invariant in time and height above the bed, it can
462 be included in the instrument constant, which needs to be determined by calibration,

$$k_t'' = \left\{ \frac{3\tau c}{16} \right\}^{1/2} \frac{0.96}{ka_t} \frac{p_0}{p_{ref}}. \quad (19)$$

463 Rearranging Eqs. 18 and 19, finally the equation to estimate $M(r)$ takes the following form,

$$M(r) = \left\{ \frac{10^{I_{dB}/20} r \psi}{k_s k_t''} \right\}^2 e^{4r\alpha}. \quad (20)$$

464 Acknowledgments

465 The FLUMES experiment was funded by the Seine Aval Research Program (FLUMES2.1) and the INSU
466 EC2CO research program (FLUMES2.2). The authors thank the crew of the R/V Cte de la Manche for their
467 kind assistance during field surveys.

468 References

469 Berhane, I., Sternberg R.W., Kineke G.C., Milligan T.G., Kranck, K., 1997. The variability of suspended
470 aggregates on the Amazon Continental Shelf. *Continental Shelf Research* 17, 267-285.

- 471 Betteridge, K. F. E., P. D. Thorne, and R. D. Cooke (2008), Calibrating multi-frequency acoustic backscatter
472 systems for studying near-bed suspended sediment transport processes, *Cont. Shelf Res.*, 28, 227–235.
- 473 Brenon, I., and P. Le Hir (1999), Modelling the turbidity maximum in the Seine estuary (France): identifi-
474 cation of formation processes, *Estuar. Coast. Shelf Sci.*, 49 (4), 525–544
- 475 Crawford, A.M., and A.E. Hay (1993), Determining suspended sand size and concentration from multifre-
476 quency acoustic backscatter, *J. Acoust. Soc. Am.*, 94 (6), 2247-2254.
- 477 Deines, K. L. (1999), Backscatter estimation using broadband acoustic Doppler current profilers, *Proc. Sixth*
478 *Working Conf. on Current Measurement*, San Diego, CA, IEEE, 249–253.
- 479 Deloffre, J., R. Lafite, P. Lesueur, R. Verney, S. Lesourd, A. Cuvilliez, and J. Taylor (2006), Controlling
480 factors of rhythmic sedimentation processes on an intertidal estuarine mudflat. Role of the turbidity max-
481 imum in the macrotidal Seine estuary, France, *Mar. Geol.*, 255, 151–164.
- 482 Downing, A., P.D. Thorne, and C.E. Vincent (1995), Backscattering from a suspension in the near field of a
483 piston transducer, *J. Acoust. Soc. Am.*, 97 (3), 1614-1620.
- 484 Dyer, K. R., 1989. Sediment processes in estuaries: future research requirements. *Journal of Geophysical*
485 *Research* 97, 14327–14339.
- 486 Dyer, K. R., and A.J. Manning (1999), Observation of size, settling velocity and effective density of flocs,
487 and their fractal dimensions, *J. Sea Res.*, 41, 87-95.
- 488 Francois, R.E., and G.R. Garrison (1982), Sound absorption based on ocean measurements. Part I: pure
489 water and magnesium sulfate contributions, *J. Acoust. Soc. Am.*, 72, 896-907.
- 490 Fugate, D.C., and C.T. Friedrichs (2002), Determining concentration and fall velocity of estuarine particle
491 populations using ADV, OBS and LISST, *Cont. Shelf Res.*, 22, 1867-1886.
- 492 Gartner, J.W. (2004), Estimating suspended solids concentrations from backscatter intensity measured by
493 acoustic Doppler current profiler in San Francisco Bay, California, *Mar. Geol.*, 211, 169-187.
- 494 Gostiaux, L., and H. (2010), Extracting meaningful information from uncalibrated backscattered echo in-
495 tensity data, *Journal of Atmospheric and Oceanic Technology*, 27, 943–949.

- 496 Guezenc, L., R. Lafite, J.-P. Dupont, R. Meyer, and D. Boust (1999), Hydrodynamics of suspended par-
497 ticulate matter in the tidal freshwater zone of a macrotidal estuary (the Seine estuary, France), *Estuaries*,
498 22:717–727.
- 499 Ha, H.K., W.-Y. Hsu, J.-Y. Maa, Y. Shao, and C. Holland (2009), Using ADV backscatter strength for
500 measuring suspended cohesive sediment concentration, *Cont. Shelf Res.*, 29 (10), 1310–1316.
- 501 Ha, H.K., J.P. -Y. Maa, K. Park, and Y.H. Kim (2011), Estimation of high-resolution sediment concentration
502 profiles in bottom boundary layer using pulse-coherent acoustic Doppler current profiles, *Mar. Geol.*, 279
503 (2011), 199-209.
- 504 Hay, A.E., and J. Sheng (1992), Vertical Profiles of Suspended Sand Concentration and Size From Multifre-
505 quency Acoustic Backscatter, *J. Geophys. Res. Oceans*, 97, C10, doi:10.1029/92JC01240.
- 506 Hill, P.S., G. Voulgaris, and J.H. Trowbridge (2001), Controls on floc size in a continental shelf bottom
507 boundary layer. *J. Geophys. Res.*, 106, C5, 9543-9549.
- 508 Hoitink, A.J.F., and P. Hoekstra (2005), Observations of suspended sediment from ADCP and OBS mea-
509 surements in a mud-dominated environment, *Coastal Eng.*, 52, 103–118.
- 510 Holdaway, G.P., Thorne P. D., Flatt D., Jones S.E., Prandle D., 1999. Comparison between ADCP and
511 transmissometer measurements of suspended sediment concentration. *Cont. Shelf Res.*, 19, 421-441.
- 512 Kaye, G.W.C., and T.H. Laby (1986), Tables of physical and chemical constants. Longman, UK, pp. 477.
- 513 Kim, Y.H., Gutierrez, B., Nelson, T., Dumars, A., Maza, M., Perales, H., Voulgaris, G. (2004), Using
514 the acoustic Doppler current profiler (ADCP) to estimate suspended sediment concentration. Technical
515 Report CPSD #04-01, Department of Geological Sciences, University of South Carolina, SC, 20 p.
- 516 Kineke G.C., and R.W. Sternberg (1992), Measurements of high concentration suspended sediments using
517 the optical backscatterance sensor, *Mar. Geol.*, 108 (3-4): 253-258.
- 518 Kranenburg, C. (1994), On the fractal structure of cohesive sediment aggregates, *Estuar. Coas. Shelf Sci.*,
519 39, 451-460.

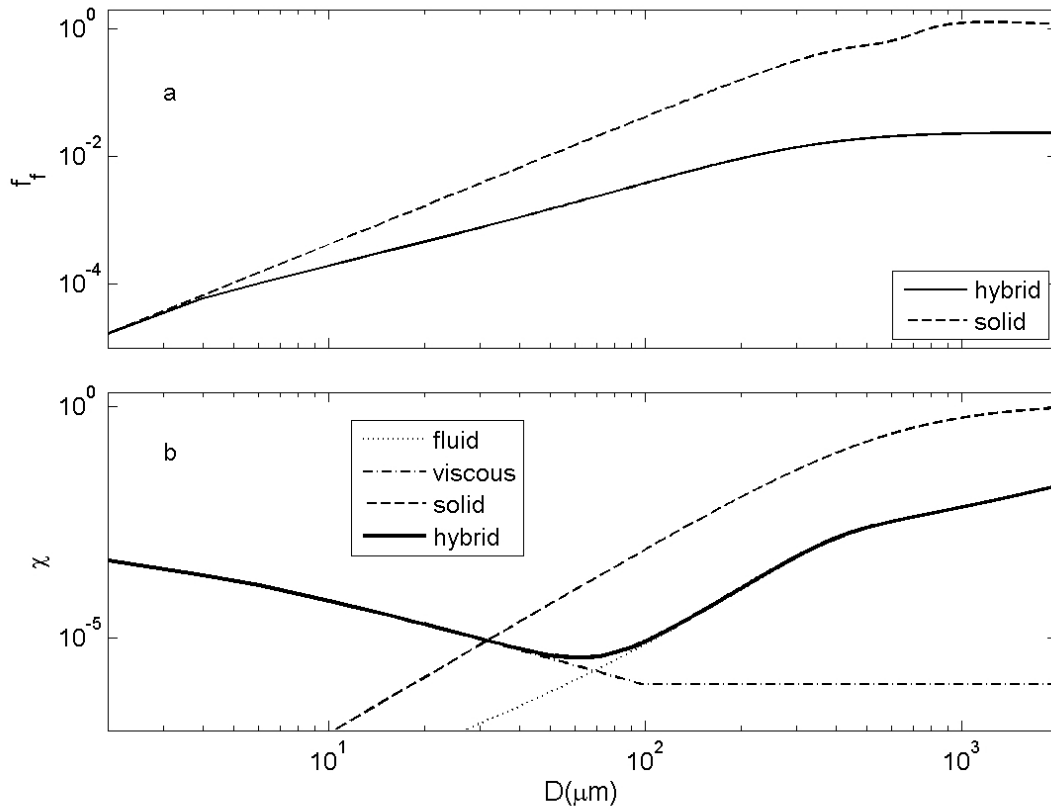
- 520 Lacy, J.R., Sherwood, C.R., Wilson, D.J., Chisholm, T.A., Gelfenbaum, G.R., 2005. Estimating hydro-
521 dynamic roughness in a wave-dominated environment with a high-resolution acoustic Doppler profiler.
522 *Journal of Geophysical Research* 110, C06014, doi: 10.1029/2003JC001814.
- 523 Le Hir, P., A. Ficht, R. Silva Jacinto, P. Lesueur, J.-P. Dupont, R. Lafite, I. Brenon, B. Thouvenin, and P.
524 Cugier (2001), Fine sediment transport and accumulations at the mouth of the Seine Estuary (France),
525 *Estuaries*, 24(6B), 950–963.
- 526 Lynch, J.F., J.D. Irish, C.R. Sherwood and Y.C. Agrawal (1994), Determining suspended sediment particle
527 size information from acoustical and optical backscatter measurements, *Cont. Shelf Res.*, 14, 1139–1165.
- 528 MacDonald, I.T., C.E. Vincent, P.D. Thorne, and P.D. Moate (2013), Acoustic scattering from a suspension
529 of flocculated sediments, *J. Geophys. Res. Oceans*, 118, 1–14, <http://dx.doi.org/10.1002/jgrc.20197>.
- 530 McAnally, W.H., and A. Mehta, (2000), Aggregation rate of fine sediment, *J. Hydraul. Eng.*, 126, 883–892.
- 531 McCave, I.N. (1984), Size spectra and aggregation of suspended particles in the deep ocean, *Deep-Sea Res*
532 31:329–352
- 533 Moate, B.D., and P.D. Thorne (2013), Scattering from suspended sediments having different and mixed min-
534 eralogical compositions: comparison of laboratory measurements and theoretical predictions, *J. Acoust.*
535 *Soc. Am.*, 133 (3), 1320-1334.
- 536 Moore, S.A., J. Le Coz, D. Hurther, and A. Paquier (2012), On the application of horizontal ADCPs to
537 suspended sediment transport surveys in rivers, *Cont. Shelf Res.*, 46, 50–63.
- 538 Rouhnia, M., A. Keyvani, and K. Strom (2014), Do changes in the size of mud flocs affect
539 the acoustic backscatter values recorded by a Vector ADV?, *Cont. Shelf Res.*, 84, 84-92, doi:
540 10.1016/j.csr.2014.05.015
- 541 Safak, I., A. Sheremet, M. A. Allison, T. J. Hsu (2010), Bottom turbulence on the muddy Atchafalaya Shelf,
542 Louisiana, USA, *J. Geophys. Res. Oceans*, 115, doi:10.1029/2010JC006157.
- 543 Safak, I., M.A. Allison, and A. Sheremet (2013), Flocc variability under changing turbulent
544 stresses and sediment availability on a wave energetic muddy shelf, *Cont. Shelf Res.*, 53, 1–10,
545 <http://dx.doi.org/10.1016/j.csr.2012.11.015>.

- 546 Sahin, C., I. Safak, T.-J. Hsu, and A. Sheremet (2013), Observations of suspended sedi-
547 ment stratification from acoustic backscatter in muddy environments, *Mar. Geol.*, 336, 24-32,
548 <http://dx.doi.org/10.1016/j.margeo.2012.12.001>.
- 549 Sahin, C. (2014), Investigation of the variability of floc sizes on the Louisiana Shelf using acoustic estimates
550 of cohesive sediment properties, *Mar. Geol.*, 353, 55-64, <http://dx.doi.org/10.1016/j.margeo.2014.03.022>.
- 551 Sheng, J., and A.E. Hay (1988), An examination of the spherical scatter approximation in aqueous suspen-
552 sions of sand, *J. Acoust. Soc. Am.*, 83, 598-610.
- 553 Shields, F. D. (2010), Aquatic habitat bottom classification using ADCP, *J. Hydraul. Eng.*, 136, 336-342,
554 [doi:10.1061/\(ASCE\)HY.1943-7900.0000181](https://doi.org/10.1061/(ASCE)HY.1943-7900.0000181).
- 555 Thorne, P. D., C. E. Vincent, P. J. Harcastle, S. Rehman and N. Pearson (1991), Measuring suspended
556 sediment concentrations using acoustic backscatter devices, *Mar. Geol.*, 98, 7-16.
- 557 Thorne, P.D., P.J. Harcastle, and R.L. Soulsby (1993), Analysis of acoustic measurements of suspended
558 sediments, *J. Geophys. Res. Oceans*, 98 (C1), 899-910.
- 559 Thorne, P. D. and P. J. Harcastle (1997), Acoustic measurements of suspended sediments in turbulent
560 currents and comparison with in-situ samples, *J. Acoust. Soc. Am.*, 101, 2603-2614.
- 561 Thorne, P.D., and D.M. Hanes (2002), A review of acoustic measurement of small-scale sediment processes,
562 *Cont. Shelf Res.*, 22, 603-632.
- 563 Thorne, P.D., and R. Meral (2008), Formulations for the scattering properties of suspended sandy sediments
564 for use in the application of acoustics to sediment transport processes. *Cont. Shelf Res.*, 28, 309-317.
- 565 Thorne, P.D., I.T. MacDonald, and C.E. Vincent (2014), Modelling acoustic scattering by suspended floc-
566 culating sediments, *Cont. Shelf Res.*, in press, <http://dx.doi.org/10.1016/j.csr.2014.07.003>.
- 567 Uncles, R.J., J.A. Stephens, and R.E. Smith (2002), The dependence of estuarine turbidity on tidal intrusion
568 length, tidal range and residence time, *Cont. Shelf Res.*, 22 (11-13), 1835-1856.
- 569 Urlick, R.J. (1948), The absorption of sound in irregular particles, *J. Acoust. Soc. Am.*, 20 (3), 283-289.

- 570 Verney, R., R. Lafite, and J. Brun-Cottan (2009), Flocculation potential of estuarine particles: The impor-
571 tance of environmental factors and of the spatial and seasonal variability of suspended particulate matter,
572 *Estuar. Coast.*, 32, 678-693.
- 573 Verney, R., R. Lafite, J.C. Brun-Cottan, and P. Le Hir (2011), Behaviour of a floc population during
574 a tidal cycle: Laboratory experiments and numerical modelling, *Cont. Shelf Res.*, 31, S64-S83, doi:
575 10.1016/j.csr.2010.02.005.
- 576 Verney, R., G. Voulgaris, A. Manning, J. Deloffre, and P. Bassoullet (2013), Quantifying suspended partic-
577 ulate matter (SPM) dynamics in estuaries: combining acoustic and optical approaches, *Proceedings of*
578 *the International Conference on Cohesive Sediment Transport Processes (INTERCOH)*, October 2013,
579 Gainesville, Florida.
- 580 Vincent C.E., and I.T. MacDonald (2015), A flocculi model for the acoustic scattering from flocs, *Cont.*
581 *Shelf Res.*, 104, 15-24, <http://dx.doi.org/10.1016/j.csr.2015.05.002>
- 582 Voulgaris, G., and S. Meyers (2004), Temporal variability of hydrodynamics, sediment concentration and
583 sediment settling velocity in a tidal creek, *Cont. Shelf Res.*, 24, 1659-1683.
- 584 Wang, Y. P., G. Voulgaris, Y. Li, Y. Yang, J. Gao, J. Chen, and S. Gao (2013), Sediment resuspen-
585 sion, flocculation, and settling in a macrotidal estuary, *J. Geophys. Res. Oceans*, 118, 5591–5608,
586 doi:10.1002/jgrc.20340.
- 587 Winterwerp, J. C. (2002), On the flocculation and settling velocity of estuarine mud, *Cont. Shelf Res.*, 22,
588 1339-1360, doi:10.1016/S0278-4343(02)00010-9.

Date (2011)	Tidal range (m)
May 18th	7.00
May 23rd	5.05
November 3rd	3.45
November 10th	5.85

Table 1: Tidal ranges for different data sets

Figure 1: Variation of (a) the form function, f_f , and (b) the normalized total scattering cross section, χ , with particle size for a solid, fluid and hybrid scatterer.

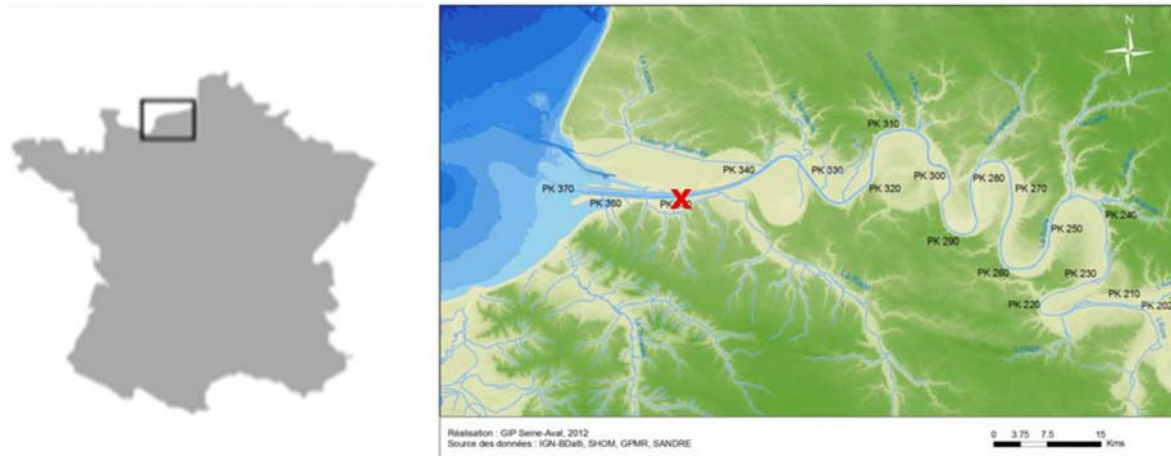


Figure 2: The approximate location of the sampling station (red 'x') in the lower reaches of the Seine estuary, France (49.4365° latitude North, 0.3187° longitude East).

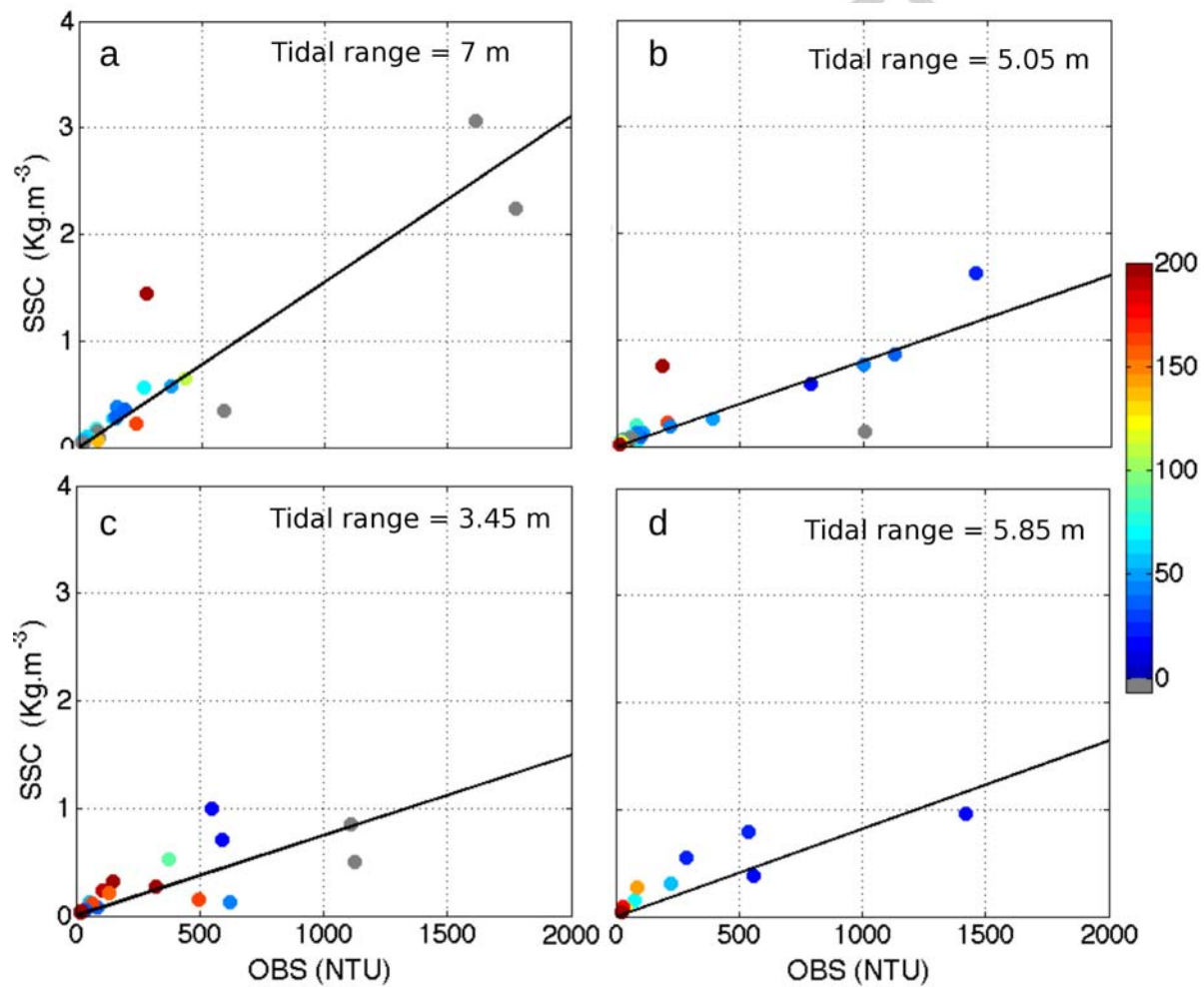


Figure 3: Calibration of the OBS for different data sets: (a) May 18th, (b) May 23rd, (c) November 3rd, (d) November 10th. Colorbar indicates the floc sizes. Gray points correspond to the data with no floc size information available.

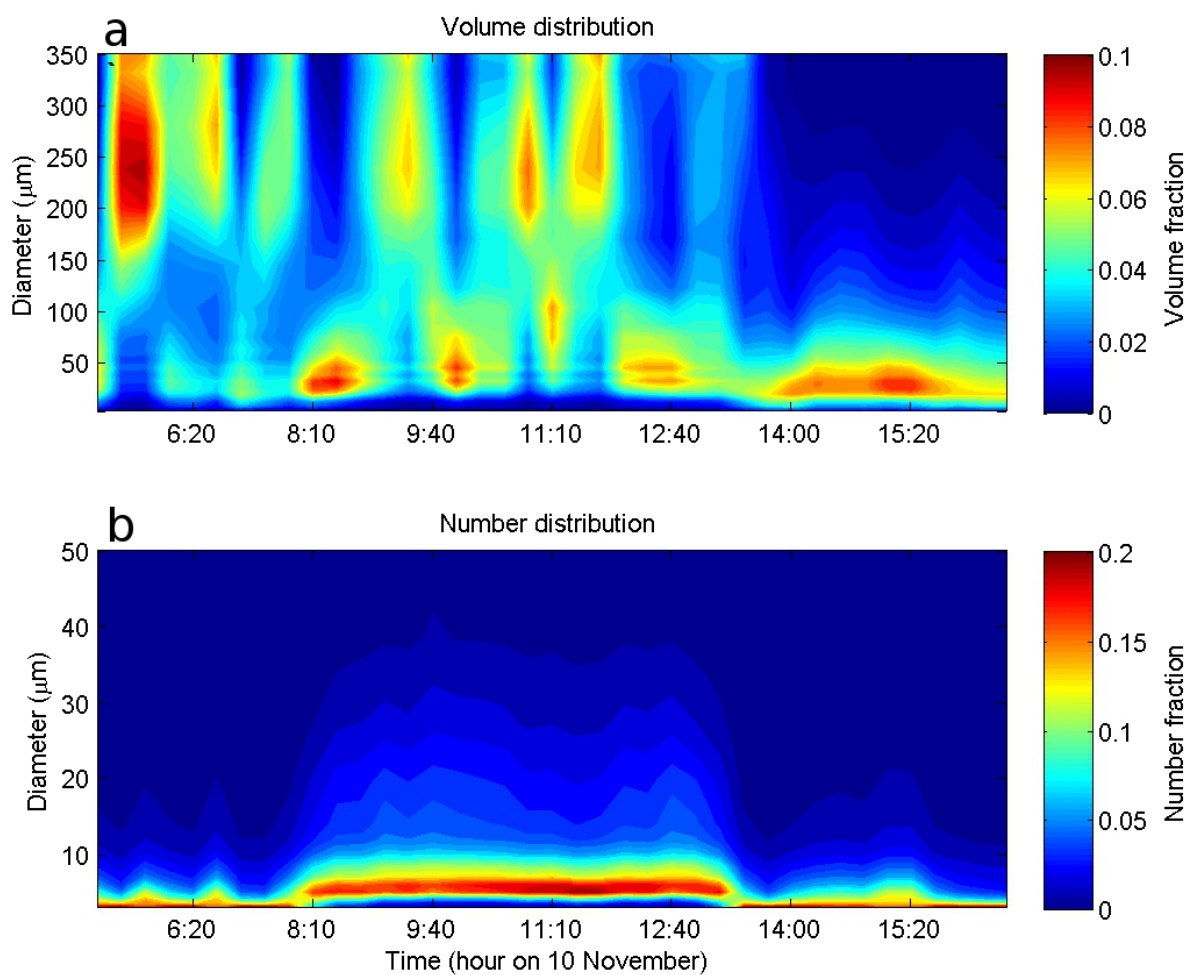


Figure 4: Example of grain size distributions measured by the LISST (November 10th) represented as (a) volume fraction and (b) number fraction distributions. The distributions show the normalized values, rather than the units micro-litres and numbers of particles per liter.

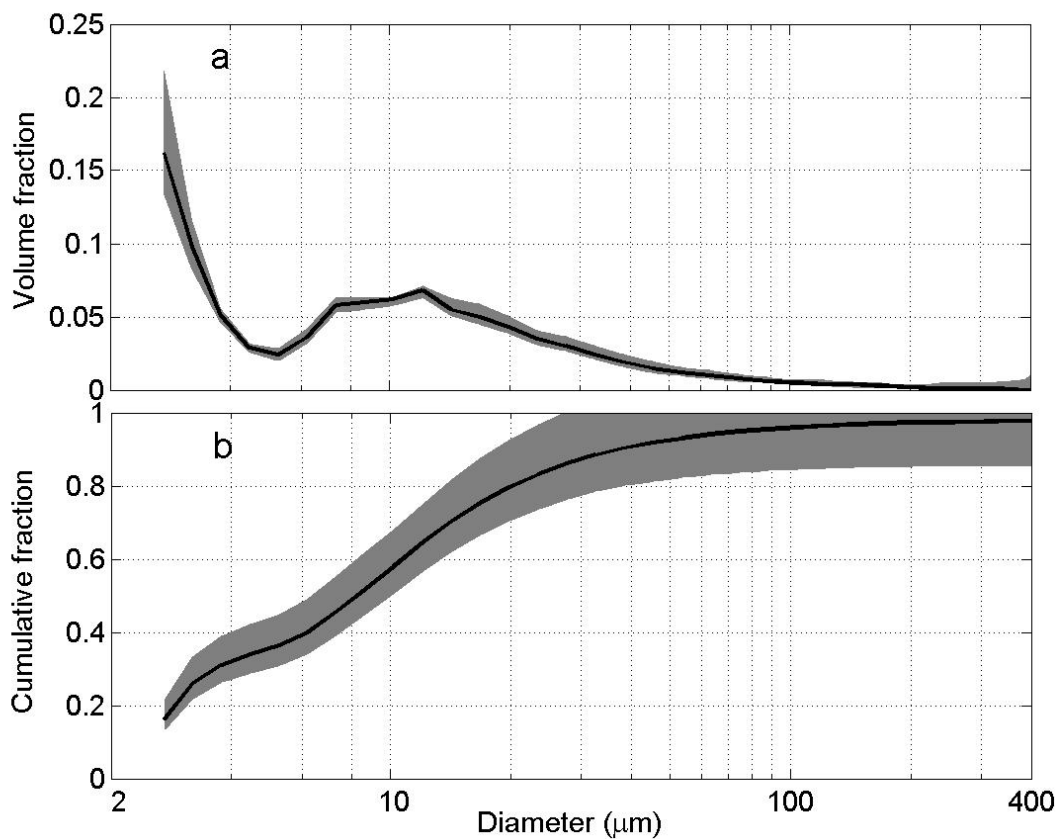


Figure 5: An example of a de-flocculated particle size distributions (based on samples taken on May 18th), (a) volume fraction and (b) cumulative fraction distributions. Black solid lines represent the median of all samples per size classes. Upper and lower limits of gray shades correspond to 10th and 95th percentiles, respectively.

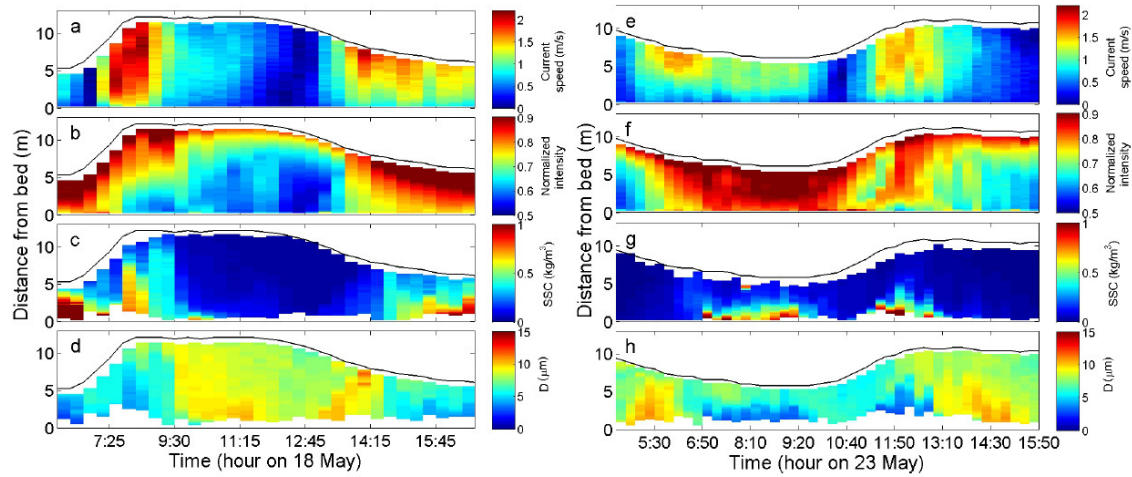


Figure 6: Observations during Spring (left panel) and Neap (right panel) tides in May 2011. Vertical structure of (a,e) mean current recorded by the ADCP, (b,f) normalized ADCP acoustic backscatter intensity, (c,g) suspended sediment concentration measured by the OBS, (d,h) mean floc size over the particle number size distribution measured by the LISST.

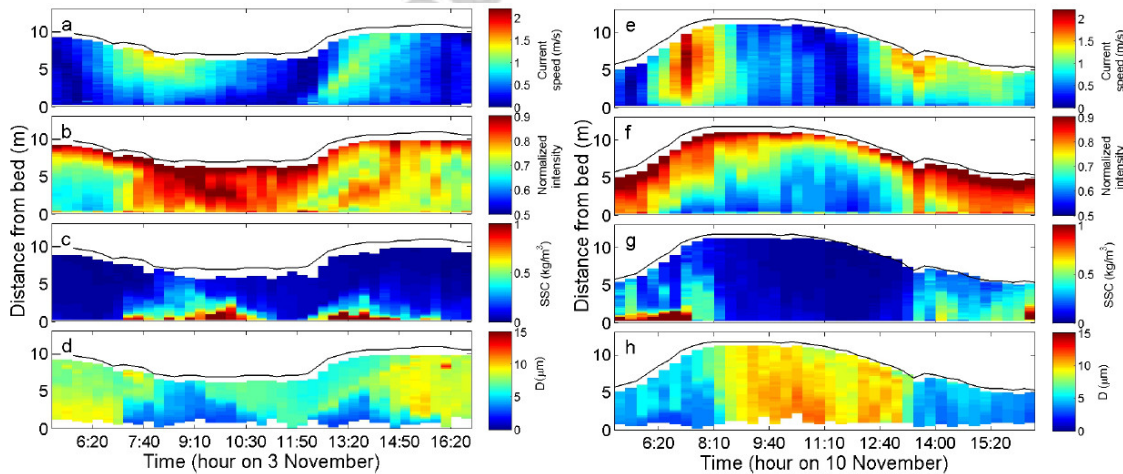


Figure 7: Observations during Neap (left panel) and Spring (right panel) tides in November 2011. Vertical structure of (a,e) mean current recorded by the ADCP, (b,f) normalized ADCP acoustic backscatter intensity, (c,g) suspended sediment concentration measured by the OBS, (d,h) mean floc size over the particle number size distribution measured by the LISST.

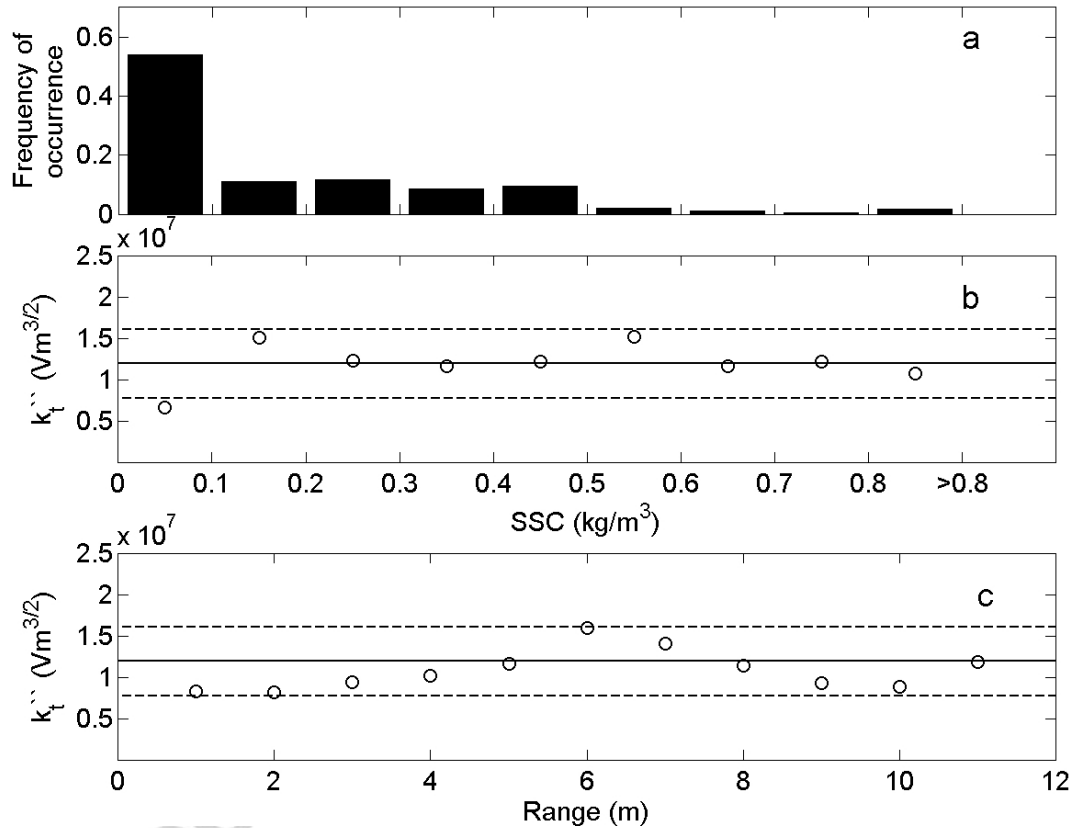


Figure 8: (a) The histogram of suspended sediment concentration observations. (b) Variation of k_t with suspended sediment concentration. (c) Variation of k_t with the range from the instrument. The solid line mark the averaged k_t values over the all concentration classes, and the dashed lines are $\pm 30\%$ difference from the average value.

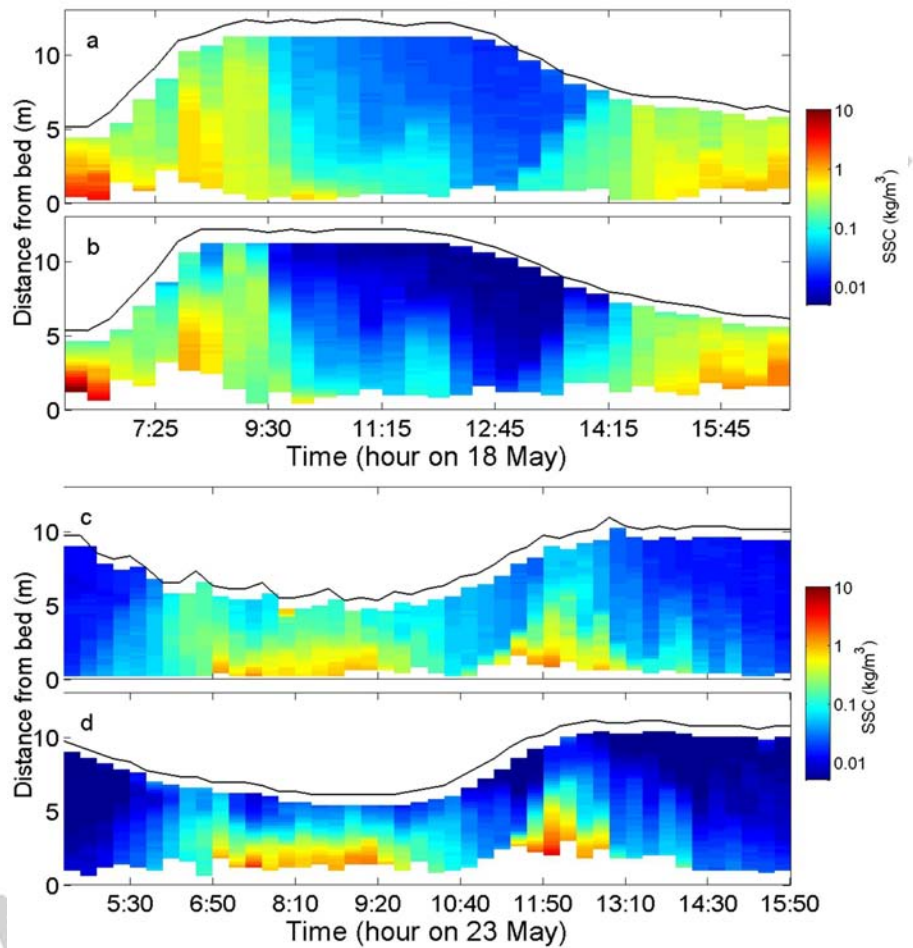


Figure 9: Evolution of SSC vertical structures (a,c) measured by the OBS and (b,d) estimated from ADCP backscatter using the measured floc sizes in May 2011. The panels share the same color bar.

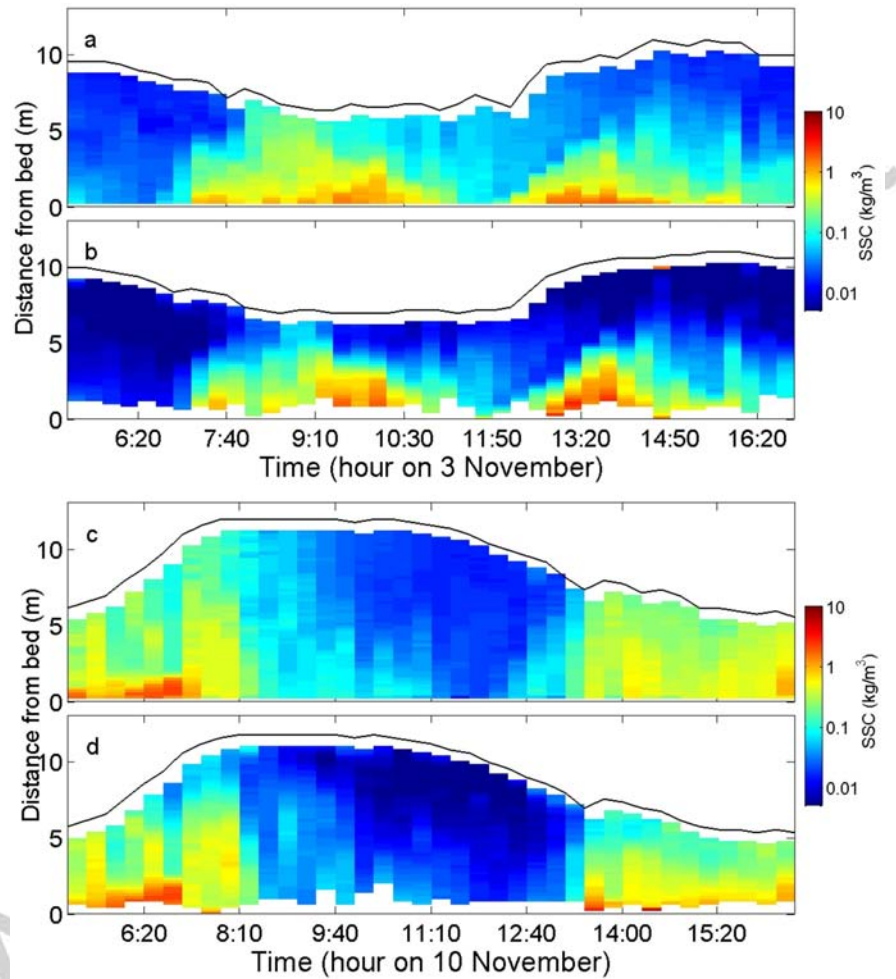


Figure 10: Evolution of SSC vertical structures (a,c) measured by the OBS and (b,d) estimated from ADCP backscatter using the measured floc sizes in November 2011. The panels share the same color bar.

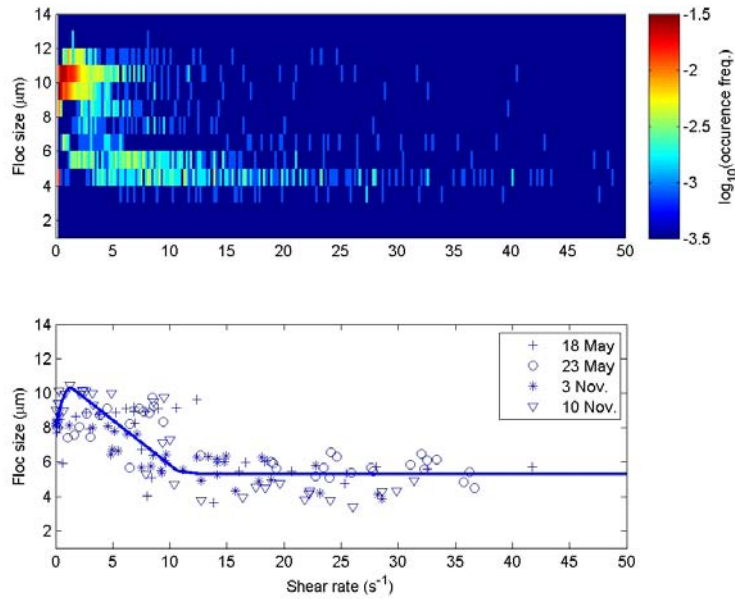


Figure 11: (a) Occurrence frequencies surface for different shear rate-floc size (D_{mn}) pairs. (b) Relationship between the vertically averaged shear rates and mean floc sizes (D_{mn}). Solid line represent the combination of linear regression lines for different turbulence conditions.

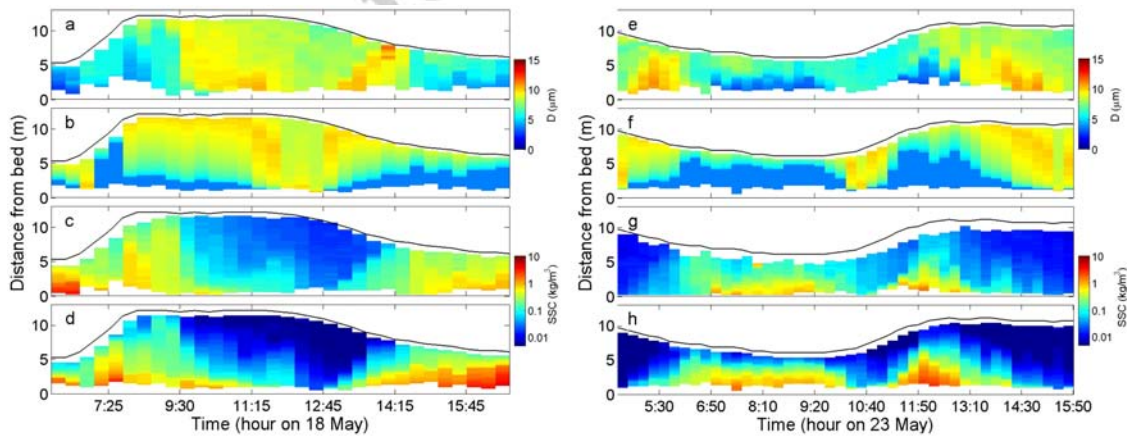


Figure 12: Comparisons during Spring (left panel) and Neap (right panel) tides in May 2011. Vertical structure of (a,e) mean floc sizes over the particle number size distributions measured by the LISST (b,f) mean floc size estimates, (c,g) suspended sediment concentration measured by the OBS, (d,h) suspended sediment concentration estimates using the estimated floc sizes.

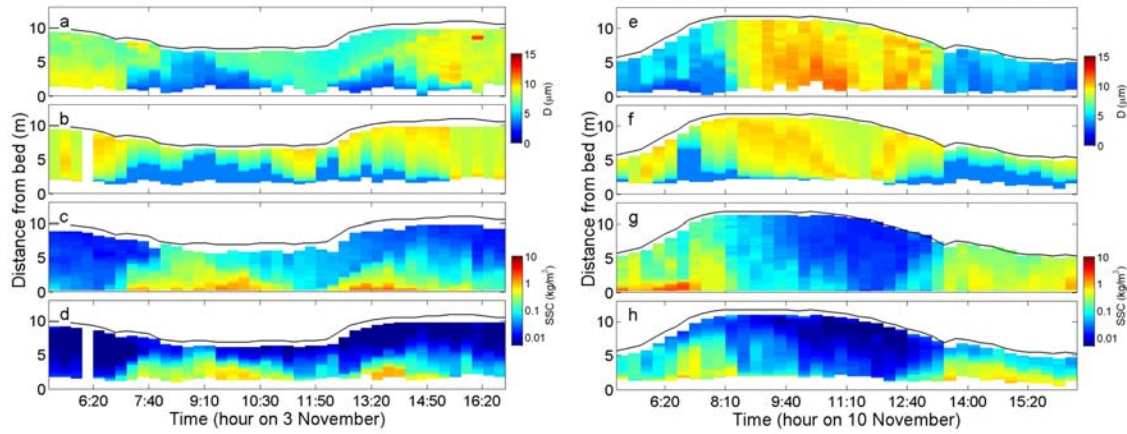


Figure 13: Comparisons during Neap (left panel) and Spring (right panel) tides in November 2011. Vertical structure of (a,e) mean floc sizes over the particle number size distributions measured by the LISST (b,f) mean floc size estimates, (c,g) suspended sediment concentration measured by the OBS, (d,h) suspended sediment concentration estimates using the estimated floc sizes.

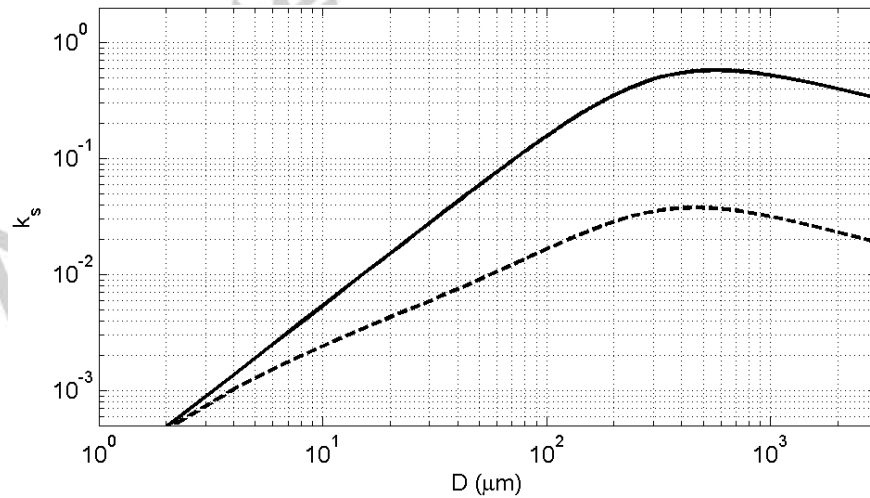


Figure 14: Variation of the sediment backscattering property, k_s , with sediment diameter (black: solid particle-scatterer model, dashed: floc-scatterer model).

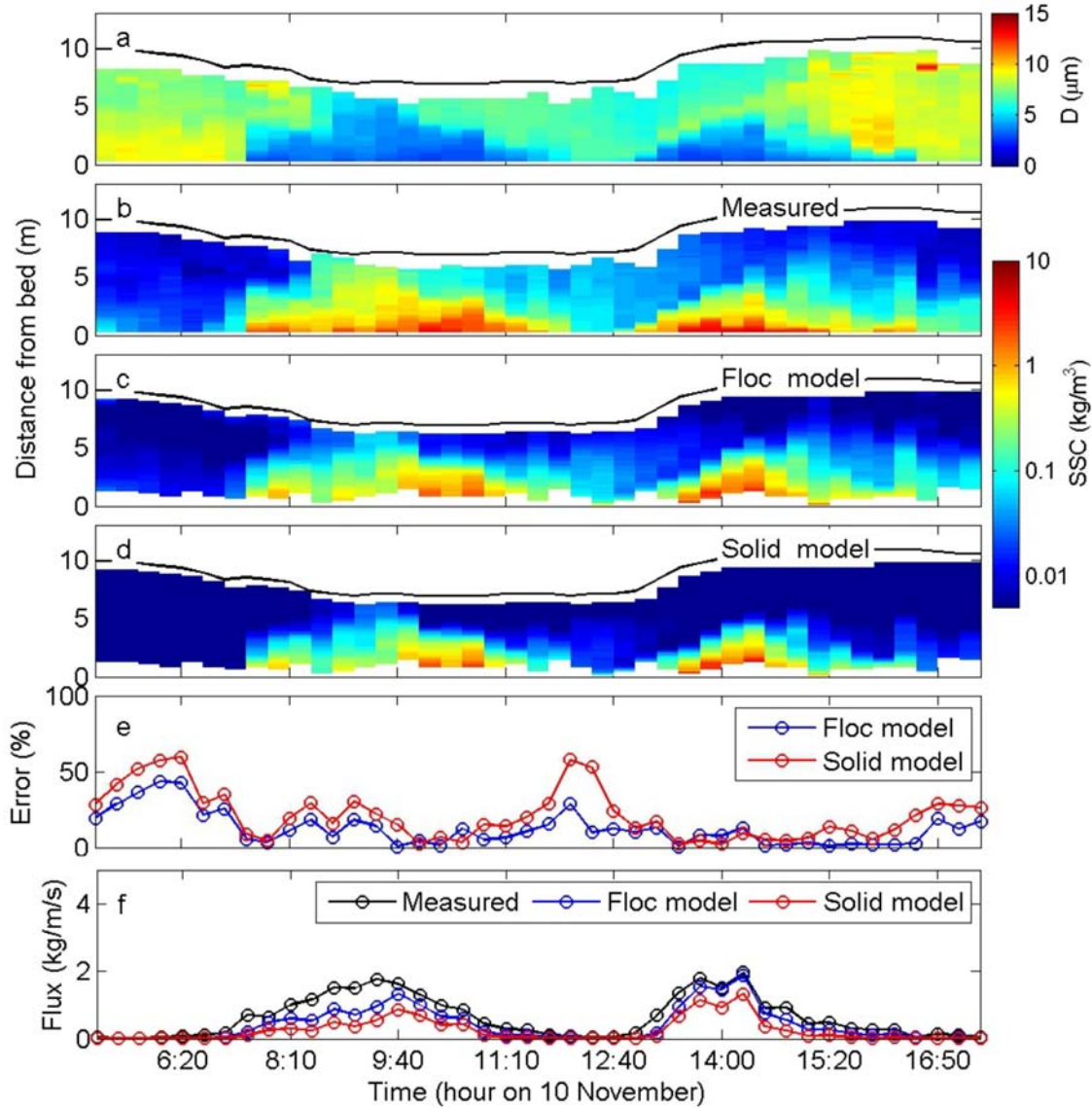


Figure 15: Comparisons during Neap tide in November 2011. Vertical structure of (a) mean floc sizes over the particle number size distributions measured by the LISST, (b) suspended sediment concentration measured by the OBS, (c) suspended sediment concentration estimates using the floc-scatterer (hybrid) model, (d) suspended sediment concentration estimates using the solid particle-scatterer model. (e) Evolution of the percentage errors for the floc-scatterer (hybrid) model and the solid particle-scatterer model. The model results are based on the measured particle sizes.

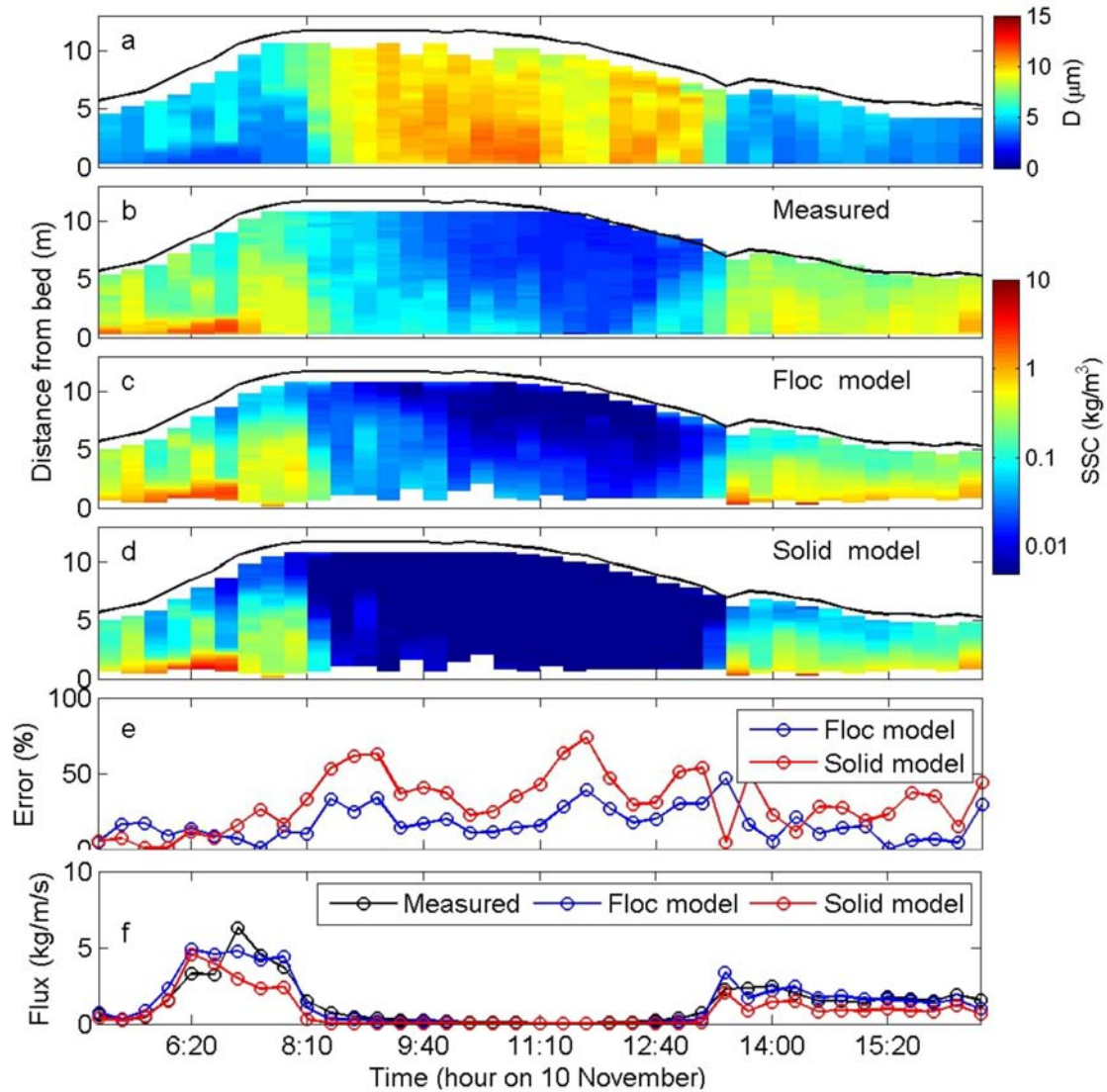


Figure 16: Comparisons during Spring tide in November 2011. Vertical structure of (a) mean floc sizes over the particle number size distributions measured by the LISST, (b) suspended sediment concentration measured by the OBS, (c) suspended sediment concentration estimates using the floc-scatterer (hybrid) model, (d) suspended sediment concentration estimates using the solid particle-scatterer model. (e) Evolution of the percentage errors for the floc-scatterer (hybrid) model and the solid particle-scatterer model. The model results are based on the measured particle sizes.

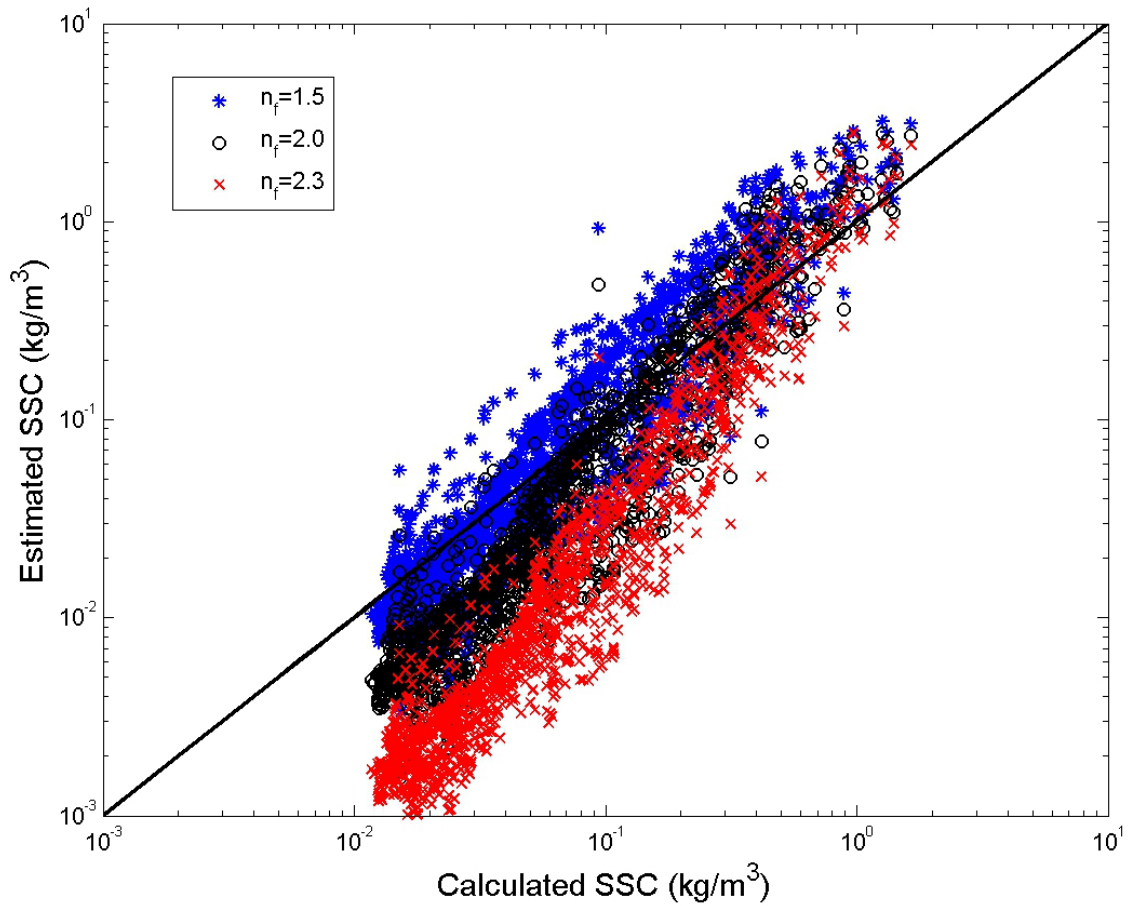


Figure 17: Correlation between measured (OBS) and estimated (ADCP) suspended sediment concentrations during Neap tide in November 2011 (red \times : estimates using $n_f=2.3$, black \circ : estimates using $n_f=2$, blue $*$: estimates using $n_f=1.5$).